Li3V2(PO4)3 cathode materials for lithium-ion batteries : a review

Rui, Xianhong; Yan, Qingyu; Skyllas-Kazacos, Maria; Lim, Tuti Mariana

2014

Rui, X., Yan, Q., Skyllas-Kazacos, M., & Lim, T. M. (2014). Li3V2(PO4)3 cathode materials for lithium-ion batteries: A review. Journal of Power Sources, 258, 19-38.

https://hdl.handle.net/10356/104510

https://doi.org/10.1016/j.jpowsour.2014.01.126

Graphical Absrtact (for review)

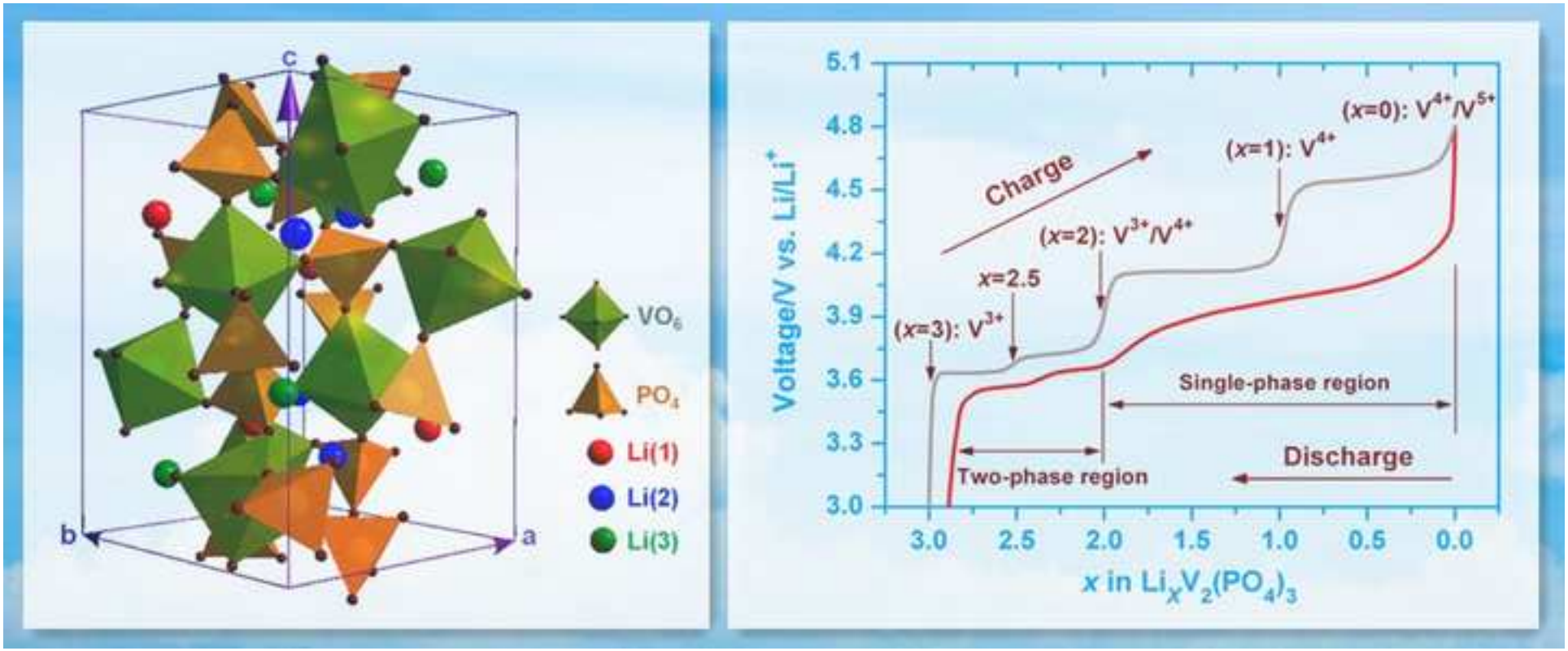

$Li_3V_2(PO_4)_3$ Cathode Materials for Lithium-Ion Batteries: A Review

Xianhong Rui,[a,b,c] Qingyu Yan,[a,c,d,*] Tuti Mariana Lim,[b,e,*] and Maria Skyllas-Kazacos [f,*]

[a]School of Materials Science and Engineering, Nanyang Technological University, 639798, Singapore

[b]School of Civil and Environmental Engineering, Nanyang Technological University, 639798, Singapore

[c]Energy Research Institute, Nanyang Technological University, 637459, Singapore

[d]TUM CREATE Centre for Electromobility, Nanyang Technological University, 637459, Singapore

[e]School of Life Sciences and Chemical Technology, Ngee Ann Polytechnic, 599489, Singapore

[f]School of Chemical Engineering, The University of New South Wales, UNSW Sydney, NSW 2052, Australia

*** Corresponding author.** Tel: +65 6790 4583, +61 2 9385 4335.

E-mail addresses: E-mail addresses: Alexyan@ntu.edu.sg (Q.Y. Yan), tmlim@ntu.edu.sg (T.M. Lim), m.kazacos@unsw.edu.au (M. Skyllas-Kazacos)

Abstract: The principal challenges facing the development of lithium ion batteries (LIBs) for hybrid electric/plug-in-hybrid (HEV/PHEV) vehicles and for off-peak energy storage are cost, safety, cell energy density (voltage × capacity), rate of charge/discharge, and service life. There are exciting developments in new positive electrode (cathode) materials to replace the $LiCoO_2$ for use in the LIBs over the past decade. Monoclinic $Li_3V_2(PO_4)_3$ (LVP) with promising electrochemical properties including excellent cycling stability, high theoretical capacity (197 mAh g^{-1}), low synthetic cost, improved safety characteristic, and low environmental impact emerges as highly suitable candidate. In this review, we focus on research work related to the LVP and discuss its host structure, mechanism of lithium insertion/extraction, transport properties (*i.e.*, electronic conductivity, and lithium diffusion), synthesis and electrochemical properties. We highlight some recent development of LVP, which shows superior cycling stability and high rate capability and give some vision for the future research of LVP based electrode.

Keywords: Lithium ion battery, cathode material, lithium vanadium phosphate, stable cyclability, high rate capability

Contents

1. Introduction

Energy is of central importance in the evolution of human societies. Fossil fuels like oil, coal, and natural gas are nature's ancient energy resources. The continued combustion of non-renewable fossil fuels, however, is not only hastening the depletable resources, but is also increasingly worsening global warming and environmental issues. Consequently, energy alternatives, such as solar, wind, hydropower, and geothermal, are emerging. Although these energy resources are renewable, cost-effective, and clean, some of them significantly rely on natural conditions (*e.g.*, sunshine, rain, wind, location, *etc.*) and thus are not reliable which restrict their widespread usage. Energy storage thus becomes even more important and has received worldwide attention. Converting into chemical energy is the most convenient form to store energy [1-7]. Rechargeable (or secondary) batteries are the most successful energy storage devices that convert off-peak electricity into chemical energy and release the stored energy reversely during the on-peak period. Currently, the most popular secondary battery technologies mainly include the lead acid, nickel-metal hydride (Ni-MH), lithium-ion, and redox flow cells. Amongst them, lithium-ion batteries (LIBs) with various shapes (*e.g.*, coin, cylindrical, prismatic, or stack, *etc.*) are the dominant power sources in today's information-rich, mobile society to power numerous portable consumer electronics (*e.g.*, smartphones, tablets, notebook PCs, and camcorders, *etc.*) and even as a vital component in new hybrid electric vehicles. The motivation for using a LIB relies on its high energy density (both volumetric and gravimetric), low self-discharge rate, wide operating temperature range, no voltage depression (*i.e.*, "memory effect"), and environmental friendliness [8-14].

A typical LIB mainly consists of a negative electrode (anode) and a positive electrode (cathode) separated and connected by a Li^+ conducting electrolyte (**Fig. 1**). The first generation LIB employs the graphite as an anode, the layered $LiCoO_2$ (LCO) as a cathode, and the organic liquid of $LiPF_6$/ethylene carbonate (EC)/dimethylene carbonate (DMC) as an electrolyte [15-17]. During the electrochemical process of charging, lithium ions leave the LCO host

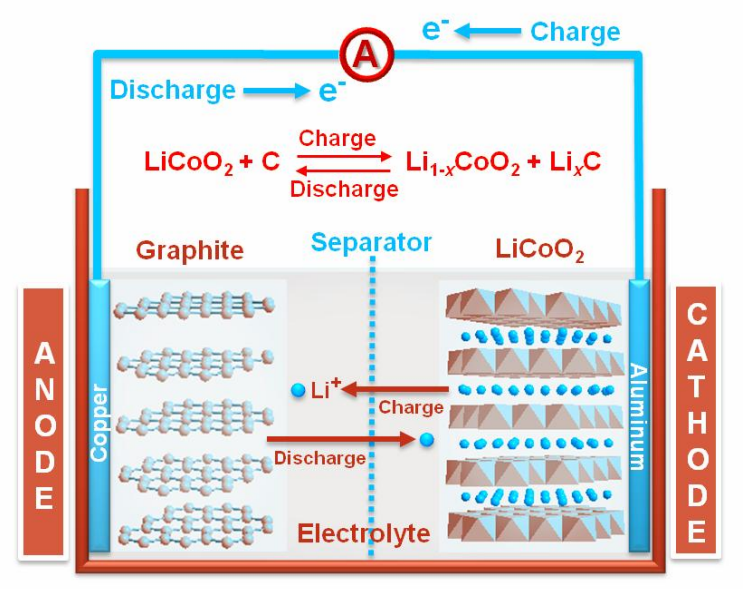

Fig. 1 Schematic illustration of a lithium ion battery employing graphite as anode and layered $LiCoO_2$ as cathode.

structure and migrate through the electrolyte to the graphite, while the associated electrons driven by an external power flow from the cathode to anode. On discharging, Li ions and electrons move reversely. The LIB performance (*e.g.*, cell potential, capacity or energy density) is largely dependent on the intrinsic chemistry of negative and positive electrode materials. The basic requirements for electrode material selection include [18-22]: (i) a high specific charge and charge density; (ii) a high (cathode) and low (anode) standard redox potential; (iii) electrochemical compatibility with the electrolyte solution; (iv) a facile electrode kinetic; (v) a high degree of reversibility; (vi) environmental benignity; (vii) safety; and (viii) moderate cost. Great achievements have been made recently in anode materials by the introduction of metals (*e.g.*, Si [23-26], Sn [27-30], Sb [31-34], Ge [35-38], *etc.*), and metal oxides (*e.g.*, SnO_2 [39-42], Fe_2O_3 [43-46], Co_3O_4 [47-51], CuO [52-54], *etc.*), which can react with a large number of lithium per formula unit and provide specific capacities more than twice of that conventional graphite (372 mAh g^{-1}). Similarly, there is a growing interest in developing high capacity cathode materials to power large-scale systems [55]. Moreover, cathodes have a significant

impact on the cell voltage, charge transfer kinetic, safety, and cost [56]. Therefore, the developments of cathode materials have become extremely important.

State-of-the-art cathode materials mainly include layered lithiated transition metal oxides (*e.g.*, LCO and $LiNi_{1-x-y}Co_xMn_yO_2$ ($0 \leq x, y \geq 1$)), Mn-based spinels (*e.g.*, $LiMn_2O_4$), vanadium pentoxides, and polyanion-type materials (*e.g.*, phosphates, borates, fluorosulphates, and silicates). **Fig. 2** compares the operating voltage and practical capacity of various cathode materials presently used in LIBs. Layered LCO is the first commercial cathode for LIBs and has received tremendous attention since its discovery in 1980 [57-61]. Although the complete removal of lithium gives a large theoretical capacity of 274 mAh g^{-1}, the $Li_{1-x}CoO_2$ structure tends to be unstable at high levels of delithiation, typically when x exceeds 0.5 [61]. Accordingly, the upper cut-off potential is generally limited to ~4.2 V (*vs.* Li/Li^+), corresponding to a practical capacity of ~140 mAh g^{-1} (around 0.5 Li per formula unit of LCO). On the other hand, cobalt is very expensive and highly toxic. Another promising layered oxide cathode is $LiNi_{1/3}Mn_{1/3}Co_{1/3}O_2$ (NMC), isotypic with LCO, because of its enhanced structural stability towards higher voltages, lower cost, and better environmental compatibility with respect to LCO [62-64]. Basically, NMC also suffers the same electrochemical issues as LCO with rapid capacity loss during cycling [65]. Spinel $LiMn_2O_4$ (LMO), possessing a potential of around 4 V (*vs.* Li/Li^+) and a theoretical capacity of 148 mAh g^{-1}, offers a low-cost and non-toxicity substitution with a high thermal stability and relatively good rate capability [66-69]. Unfortunately, it has a tremendous drawback of limited cycling behavior, especially at elevated temperatures (> 50 ^oC), owing to the dissolution of manganese into the electrolyte [70], loss of oxygen during charging [71], and Jahn-Teller distortion of Mn^{3+} [72]. These deleterious effects have been largely inhibited by substituting Mn with other metal ions [73]. A Ni-doped spinel oxide, $LiNi_{0.5}Mn_{1.5}O_4$ (LNMO), is found to be the most promising one owing to its relatively good cycling behavior and high dominant plateau at around 4.7 V (*vs.* Li/Li^+) [74-78]. It is difficult, however, to synthesize a phase-pure LNMO due to the formation of inevitable impurities

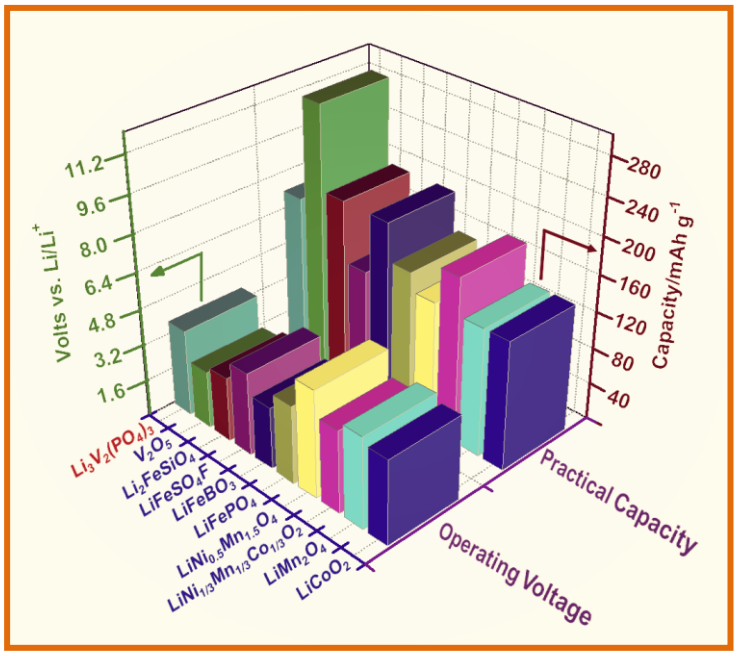

Fig. 2 Comparison of operating voltage and practical capacity of various cathode materials presently used in lithium ion batteries.

such as nickel oxides and lithium nickel oxides during the high temperature calcination [74, 79]. Besides, high voltage would cause the electrolyte decomposition resulting in the formation of unstable solid electrolyte interphase (SEI) film on the cathode side [80]. Layered vanadium pentoxides have also received much interest, which can intercalate lithium levels to achieve specific capacity of about 300 mAh g^{-1} [81-86]. Their relatively low voltages (typically around 2.5 *vs.* Li/Li^+), however, limit their applicability. Recently, in the exploring for high-performance cathode materials, polyanion compounds (*e.g.*, $LiFePO_4$ (LFP) [87], $LiFeBO_3$ [88], $LiFeSO_4F$ [89-91], and Li_2FeSiO_4 [92-95], *etc.*), possessing high thermal stability, offer particularly interesting possibilities for large-scale next-generation LIB applications. Among them, olivine LFP attracts a lot of attention, offering a theoretical capacity of 170 mAh g^{-1} and a flat voltage plateau at around 3.4 V (*vs.* Li/Li^+) [96-104]. Although great progress has been made in LFP, its redox potential is relatively low,

showing similar gravimetric energy density to LCO. Therefore, a significant research effort has been devoted to develop other phosphates with high operating voltages, such as $LiMnPO_4$ (~4.1 V *vs.* Li/Li^+) [105], $LiCoPO_4$ (~4.8 V *vs.* Li/Li^+) [106], $LiNiPO_4$ (~5.2 V *vs.* Li/Li^+) [107], and $Li_3V_2(PO_4)_3$ (LVP, ~3.8 V (average) *vs.* Li/Li^+) [108]. Monoclinic LVP with the highest theoretical capacity of 197 mAh g^{-1} (**Fig. 2**) among these high-voltage phosphate cathodes is particularly attractive due to abundant resources, safety, and rapid ionic diffusion [109]. Thus, LVP is becoming a hot research topic recently for high-energy LIBs.

Herein, we present a review specifically on the recent development of monoclinic LVP cathode materials for LIB applications. Host structure, mechanism of lithium insertion/extraction, transport properties (*i.e.*, electronic conductivity, and lithium diffusion), synthesis methods and electrochemical properties in terms of rate capability and cyclic stability are summarized and analyzed. An insight into the future research and development of LVP compound is also discussed.

2. Host structures

$Li_3V_2(PO_4)_3$ exists in two frameworks: the rhombohedral or NASICON (sodium superionic conductor) phase [110-112], and the thermodynamically more stable monoclinic form [113], differing by the way in which the "lantern" units $[V_2(PO_4)_3]$ are interconnected. The NASICON-type LVP (space group $R\bar{3}$; a = 8.316(1) Å, and c = 22.484(1) Å [114]) framework shown in **Fig. 3A**, isotypic with those of its iron, titanium, chromium, and indium analogues [115-119], consists of VO_6 octahedra and PO_4 tetrahedra connected through their vertices, forming $[V_2(PO_4)_3]$ "lantern" units stacked along the [001] direction. Lithium is located on a unique 4-fold coordinated crystallographic site [114].

The monoclinic LVP (space group $P2_1/n$; a = 8.605(1) Å, b = 8.591(1) Å, c = 12.038(1) Å, and β = 90.60(1)^o [120]) crystallizes in a structure similar to, but slightly more dense than, the NASICON phase [121]. The three-dimensional (3D) network is built from the slightly distorted VO_6 octahedra and PO_4 tetrahedra sharing oxygen

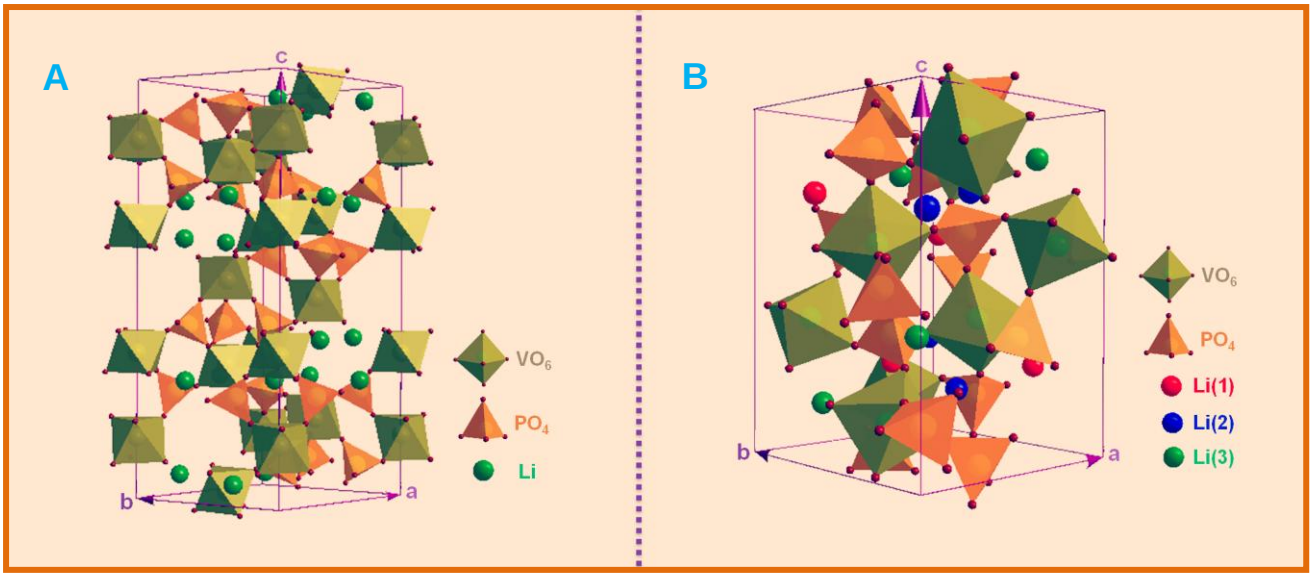

Fig. 3 Polyhedral representation of the structure of rhombohedral (A) and monoclinic (B) $Li_3V_2(PO_4)_3$.

vertexes (**Fig. 3B**) [113, 121-123]. It contains two vanadium sites V(1) and V(2) with average V-O bond lengths of 2.003 and 2.006 Å [113], respectively. Lithium atoms occupy three distinct crystallographic positions in the interstitial voids. As resolved by the ^{7}Li solid-state nuclear magnetic resonance (NMR) spectrum [113], Li(1) resides in the tetrahedral site, whereas Li(2) and Li(3) are located in two pseudotetrahedral sites (five-coordinate Li-O sites), with an additional long Li-O bond (*ca.* 2.6 Å [121]). The mobility of these three lithium sites, as determined by two-dimensional exchange spectroscopy (2D EXSY) [124], occurs on the microsecond time scale, which is much faster than the millisecond Li hopping processes in LMO [125]. On the other hand, similarly to the $Li_3Sc_2(PO_4)_3$ counterpart [126], as confirmed by differential scanning calorimetry (DSC), temperature-controlled X-ray diffraction (XRD) and Raman spectra [120, 127-129], monoclinic LVP presents three structural modifications: room temperature monoclinic α-phase, middle temperature (*ca.* 400-460 K) monoclinic β-phase, and high temperature (*ca.* 460-573 K) orthorhombic γ-phase.

These phase transitions are reversible upon cooling back to room temperature. It is noted that monoclinic LVP is not stable and undergoes oxidation of V(III) under the elevated temperature of above 800 K in air [120].

3. (De)Lithiation mechanisms

The rhombohedral and monoclinic LVP exhibit very different voltage-composition curves as a result of their structural differences. The rhombohedral LVP, that is commonly accessible by ion exchange from the corresponding sodium analogue (*i.e.*, $Na_3V_2(PO_4)_3$), displays one voltage plateau at around 3.7 V *vs.* Li/Li^+ based on the V^{3+}/V^{4+} redox couple, corresponding to a two-phase transition between the compositions of $Li_3V_2(PO_4)_3$ and $Li_1V_2(PO_4)_3$ [114, 130-132]. The monoclinic phase, where all three Li are mobile, exhibits better electrochemical properties than the rhombohedral. Thus, our review focuses on the monoclinic phase, and in the following, LVP refers to monoclinic LVP unless otherwise stated.

The electrochemical voltage-composition curve for lithium extraction/reinsertion in LVP is shown in **Fig. 4**. In the voltage range of 3.0-4.8 V *vs.* Li/Li^+ (**Fig. 4A**), there are four plateaus in the charge/oxidation curve located at around 3.6, 3.7, 4.1, and 4.6 V *vs.* Li/Li^+, corresponding to a sequence of phase transition processes between the single phases of $Li_xV_2(PO_4)_3$ (x = 3.0, 2.5, 2.0, 1.0 and 0) [113, 130, 133-135]. Li(3) (**Fig. 3B**), the highest energy site [133], is extracted firstly upon the oxidation. Meanwhile, Li(2) shifts to a tetrahedral site which is very similar to Li(1) site. The Li(3) extraction involves two steps due to the existence of an ordered phase $Li_{2.5}V_2(PO_4)_3$ [135], occurring at 3.6, and 3.7 V *vs.* Li/Li^+, which results in a V^{3+}/V^{4+} ordering state. Subsequent one Li extraction (4.1 V *vs.* Li/Li^+) corresponds to a two-phase process of $Li_2V_2(PO_4)_3 \rightarrow LiV_2(PO_4)_3$ with full oxidation of V^{3+} to V^{4+}. At this stage, as a result of the repulsion energy of the $Li(1)^+$- $V(1)^{4+}$ pair in $Li_2V_2(PO_4)_3$ [133], Li(1) is extracted. The last lithium (*i.e.*, Li(2)) extraction, at higher voltage ~4.6 V *vs.* Li/Li^+, once again as a two-phase reaction between $LiV_2(PO_4)_3$ and $V_2(PO_4)_3$, is

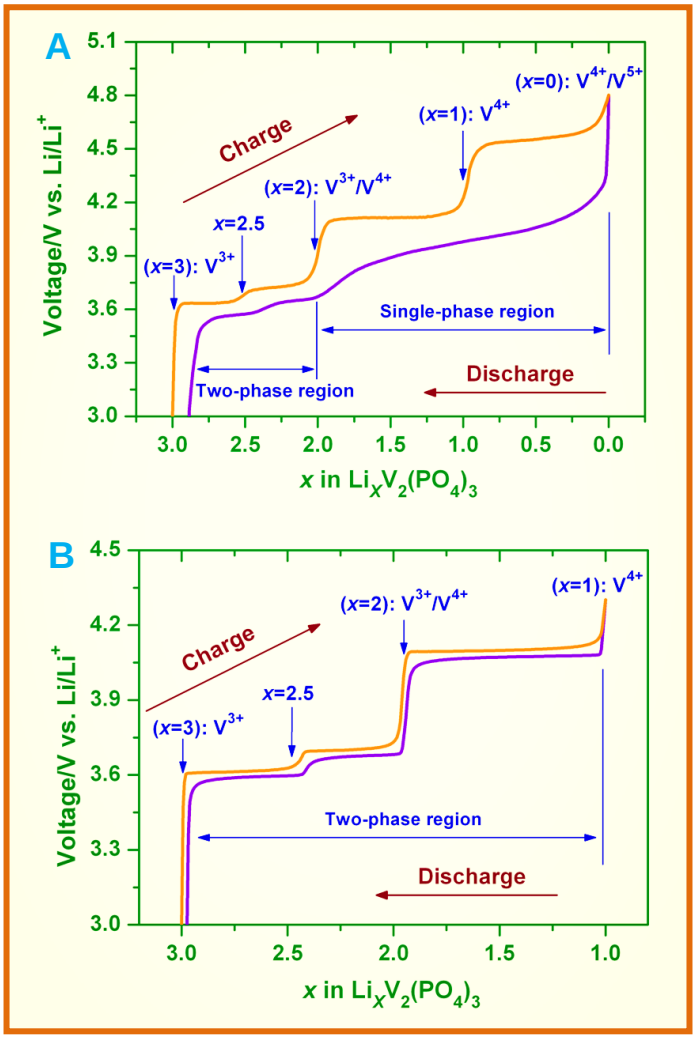

Fig. 4 The electrochemical voltage-composition curves of $Li_3V_2(PO_4)_3$ in the voltage ranges of 3.0-4.8 (A) and 3.0-4.3 (B) V *vs.* Li/Li^+.

associated with the oxidation of part of V^{4+} into V^{5+}, and is kinetically the most difficult [113] due to the reduced ionic/electronic conductivity for the fully emptied framework $V_2(PO_4)_3$. After removal of all of the lithium ions, the overall volume contraction $\Delta V/V$ is 7.8% [113], which is comparable to the 6.6% volume decrease in LFP on delithiation to $FePO_4$ [136], and hence the monoclinic symmetry is preserved for $V_2(PO_4)_3$ lattice. The structural similarity between $Li_3V_2(PO_4)_3$ and $V_2(PO_4)_3$ prevents fast capacity degradation resulting from severe volumetric

changes during the charge and discharge process. Here, it is worth mention that, in emptied $V_2(PO_4)_3$, V(1) and V(2) exhibit fairly close average bond distance and average vanadium valence (+4.5) [113], indicating that the mixed V^{4+}/V^{5+} state does not display charge ordering in this phase. Such phenomena will result in a disorder of lithium reinsertion (in the absence of V^{n+} ordering to drive Li^+ ordering), as is evident from the solid solution behavior (*i.e.*, single-phase reaction) characterized by the S-shaped curve (**Fig. 4A**) during the initial discharge process. It persists until sufficient Li^+ repopulation and vanadium reduction are attained. At the composition of $Li_2V_2(PO_4)_3$, charge ordering is reappeared, and thus two-phase behavior is reasserted in the reinsertion of the third lithium. The overall electrochemical reactions can be written as:

Charge:

$$Li_3V_2^{3+}(PO_4)_3 - 0.5Li^+ - 0.5e^- \rightarrow Li_{2.5}V^{3+}V_{1/2}^{4+}(PO_4)_3 \quad (1)$$

$$Li_{2.5}V^{3+}V_{1/2}^{4+}(PO_4)_3 - 0.5Li^+ - 0.5e^- \rightarrow Li_2V^{3+}V^{4+}(PO_4)_3 \quad (2)$$

$$Li_2V^{3+}V^{4+}(PO_4)_3 - Li^+ - e^- \rightarrow LiV_2^{4+}(PO_4)_3 \quad (3)$$

$$LiV_2^{4+}(PO_4)_3 - Li^+ - e^- \rightarrow V_2^{4.5+}(PO_4)_3 \quad (4)$$

Discharge:

$$V_2^{4.5+}(PO_4)_3 + 2Li^+ + 2e^- \rightarrow Li_2V^{3+}V^{4+}(PO_4)_3 \quad (5)$$

$$Li_2V^{3+}V^{4+}(PO_4)_3 + 0.5Li^+ + 0.5e^- \rightarrow Li_{2.5}V^{3+}V_{1/2}^{4+}(PO_4)_3 \quad (6)$$

$$Li_{2.5}V^{3+}V_{1/2}^{4+}(PO_4)_3 + 0.5Li^+ + 0.5e^- \rightarrow Li_3V_2^{3+}(PO_4)_3 \quad (7)$$

Interestingly, as shown in **Fig. 4B**, when the upper cut-off voltage drops to 4.3 V *vs.* Li/Li^+, no solid solution region is observed. The cell exhibits three charge plateaus and correspondingly three discharge plateaus, being associated with the two-phase transition processes of $Li_3V_2(PO_4)_3 \leftrightarrow Li_{2.5}V_2(PO_4)_3$ (~3.6 V *vs.* Li/Li^+), $Li_{2.5}V_2(PO_4)_3 \leftrightarrow Li_2V_2(PO_4)_3$ (~3.7 V *vs.* Li/Li^+), and $Li_2V_2(PO_4)_3 \leftrightarrow LiV_2(PO_4)_3$ (~4.1 V *vs.* Li/Li^+). As reported elsewhere [137-139], without

formation of kinetically sluggish $V_2(PO_4)_3$ phase, although the capacity is relatively low, more stable capacity retention on cycling can be observed for LVP in the voltage range of 3.0-4.3 V *vs.* Li/Li^+.

4. Transport properties

The electrochemical performances of LIBs including capacity, cycle life, and rate capability are mainly dependent on the electronic and ionic conductivities of electrode materials. Thus, information on the transport properties of LVP is important and described in the following sections.

4.1. Electronic conductivity

In phosphate-type cathode materials, although the inductive effect generated by the $(PO_4)^{3-}$ groups can raise their operating potentials relative to the oxide counterparts [87, 140], the electronically insulating phosphate groups also isolate the valence electrons of transition metals within the lattices resulting in low intrinsic electronic conductivities [97]. The pristine LVP compound shows a relatively low electronic conductivity (*e.g.*, 2×10^{-8} S cm^{-1} in [113], and 7.7×10^{-8} S cm^{-1} in [141]) as determined by the four-point-probe conductivity measurement, which is comparable to that of other lithium metal phosphates such as LFP [142], but much lower than that of LCO (~10^{-3} S cm^{-1} [143]) and LMO (~10^{-4} S cm^{-1} [144]). Approaches such as surface coating with carbon [141, 145], transition metal doping [146], or a combination of them [147] have been attempted to increase the electronic conductivity of LVP. Results show that a remarkable jump in electrical conductivity has been achieved, *e.g.*, 7.2×10^{-5} S cm^{-1} for LVP/C (2.7 wt%, weight percent) [141], and 8.6×10^{-4} S cm^{-1} for Nb-doped LVP/C (2.3 wt%) [147].

4.2. Lithium diffusion

The diffusion of lithium ions into and out of active materials is central to the operation of LIBs, which is the rate-determining step in an electrochemical reaction as compared to the electronic conduction [148]. For example, the charge/discharge rate capability, an important factor for high-power LIB application, is largely related to Li-ion diffusivity. Higher diffusivity will lead to a faster lithium insertion/extraction rate. Recently, Lee *et al.* calculated the migration energies for Li-ion diffusion along different directions in LVP on the basis of a vacancy hopping mechanism using the Mott-Littleton method [149]. **Fig. 5A** shows the possible Li^+ migration pathways in LVP. The results indicate that the migration energies (< 0.4 eV) for Li^+ movement along quasi [100] direction (*i.e.*, paths A, B, and C) are much lower than the other directions (0.8-3.7 eV), suggesting a facile lithium ion transport along the *a*-axis. Using the well-known Einstein relation of $D_{Li^+} \approx \exp(E_a/\kappa_B T)$, where E_a is the migration energy, κ_B is the Boltzmann constant, and T is the temperature, the Li^+ diffusion coefficient (D_{Li^+}) at room temperature (298 K) is calculated to be around 10^{-11} cm^2 s^{-1} in the [100] direction (E_a = ~0.4 eV).

In addition to the atomic level simulation, lithium diffusion in crystalline solid electrodes can also be determined by electrochemical techniques of cyclic voltammetry (CV), electrochemical impedance spectroscopy (EIS), and galvanostatic intermittent titration technique (GITT) at a macroscopic scale [150-152]. Taking the CV plot as an example, with increasing the scan rate, not only the redox peaks become broadening and indistinct, but also the anodic (cathodic) peaks shift to higher (lower) potentials, which are caused by a limit in ionic conductivity. An important literature carried out by Rui *et al*. [153] has been devoted to systematical analysis of Li-ion diffusivity in LVP using these techniques. Here, it is worth mention that the D_{Li^+} derived from the CV, EIS, and GITT techniques is valid only in the case of solid solutions. In the two-phase region, although the physical meaning of D_{Li^+} is incomprehensible, the calculated D_{Li^+} can be taken as an effective measure that reflects the intensity of long- and short-range interactions

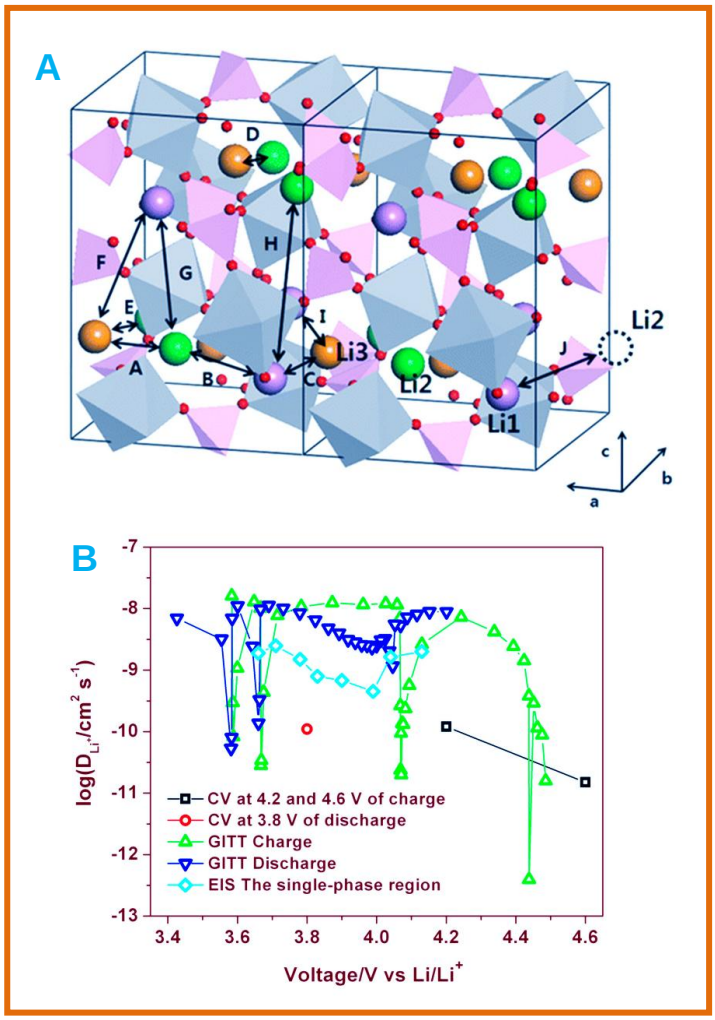

Fig. 5 (A) Possible Li-ion migration pathways in LVP. Reproduced with permission from [149]. (B) Lithium diffusion coefficients of LVP as determined by CV, GITT and EIS techniques. Reproduced with permission from [153].

between the lithium ions [150], and is known as the apparent diffusion coefficient ($D_{Li^+}^{app}$). It is found that the diffusion coefficient is closely related to the voltage states of charging and discharging as reflected by the "W" shape of D_{Li^+} -V curves in **Fig. 5B** [153]. The D_{Li^+} measured in the single-phase region ranges from 10^{-10} to 10^{-9} cm^2 s^{-1}. The $D_{Li^+}^{app}$ in the two-phase regions calculated from CV and GITT is in the ranges of 10^{-11} to 10^{-10} cm^2 s^{-1}, and 10^{-13} to 10^{-8} cm^2 s^{-1},

respectively. Besides, there are also some other reports regarding the lithium diffusion coefficient in LVP with different results [154-160]. For example, the D_{Li^+} obtained from GITT by Huang *et al*. [154] is around 10^{-9} cm^2 s^{-1} during the discharge process between 3.0 and 4.8 V *vs.* Li/Li^+. Jiang *et al*. [156] reported that the $D_{Li^+}^{app}$ in the voltage range of 3.0-4.3 V *vs.* Li/Li^+ is about 10^{-10} cm^2 s^{-1} from CV and EIS.

Apparently, the low electronic and ionic conductivities of LVP will cause slow kinetics of charge and discharge, resulting in poor rate capacity and low capacity utilization. Thus, improvement on the electronic conductivity and lithium diffusion has become the core of LVP study. Over the past few years, various approaches, such as doping with supervalent cations [161], coating conductive materials (*e.g.*, carbon) [162], scaling down the particle size [163], and tailoring the morphology and texture [164], have been explored to mitigate the drawbacks mentioned above. Therefore, in the following sections, we will introduce the synthesis methods, and benefits to the electrochemical properties of LVP in detail.

5. Synthesis

5.1. Solid state reaction

Solid-state reaction is the most common method to prepare ceramics, in which solid precursors are ground or ball-milled together, followed by heat-treatment of the resultant mixture in a furnace [165]. In the case of LVP, the raw reactants generally involve not only lithium (*e.g.*, LiF, Li_2CO_3, LiOH, or CH_3COOLi), vanadium (*e.g.*, V_2O_5, or NH_4VO_3), and phosphorous (*e.g.*, $NH_4H_2PO_4$ or $(NH_4)_2HPO_4$) sources, but also carbon-containing (*e.g.*, acetylene black) or organic compounds (*e.g.*, glucose) [123, 166-170]. After thorough mixing, the precursors are initially heated to 300-400 ^oC to expel the gases (*e.g.*, H_2O, and NH_3), and then reground and calcined at a temperature ranging from 600 to 1000 ^oC for 10-24 h under inert gas or slightly reducing atmosphere. During calcination, the carbon, be it directly

added or that formed from pyrolysis of the organic precursor, can act as a reductant to reduce V^{5+} into V^{3+}. In this manner, such synthesis approach is also known as the carbothermal reduction method. The properties of final products are closely related to the staring materials, calcination temperature and time. For example, Fu *et al*. [168] conducted a comparative study on the use of different lithium sources (LiF, and Li_2CO_3). It is found that the LVP product using LiF precursor has a lower calcination temperature (700 ^oC) and smaller particle size (around 300 nm), and thus exhibits a better electrochemical performance. They also analyzed the effect of different calcination temperatures on the performance of LVP [123]. By calcining at 750 ^oC, the impurity phase Li_3PO_4 can be detected, and at 1000 ^oC, the particles grow rather large (5-10 μm). The optimized temperature is 900 ^oC, at which the as-obtained LVP shows the particle size of 1-5 μm (**Fig. 6A**) and presents the highest initial capacity.

One disadvantage with the above solid-state reaction is long period of calcination. Recently, microwave heating has become an important sintering technique instead of furnace heating, which dramatically reduces reaction times (from days and hours to minutes and seconds) [171-174]. Besides, microwave-assisted solid-state synthesis is generally quite simpler, cleaner, and more energy efficient and economical than the conventional route. Microwave heating is a process whereby microwaves produced by magnetrons are directed toward reactants or heating medium, which absorb the electromagnetic energy volumetrically to achieve self-heating uniformly and rapidly. With these advantages, microwave solid-state method is deservedly adopted to prepare LVP cathode materials for LIBs [138, 175-177]. An early attempt at applying microwaves to synthesize LVP has been made by Yang *et al*. [138]. It is found that crystalline LVP can be rapidly synthesized at 750 ^oC for 5 min in microwave irradiation field. Compared with the electrochemical properties of the LVP sample prepared by the conventional solid-state reaction, microwave-derived LVP presents higher reversible capacity and better cycling stability.

Although the above described solid-state reactions have advantages of simple and suitable for mass production, they suffer from a series of problems, such as inhomogeneity, irregular morphology, uncontrollable particle growth and agglomeration (*i.e.*, large particle size), limiting the capacity contribution, especially at high charge/discharge rates.

5.2. Sol-gel chemistry

Sol-gel synthesis is a wet chemical approach for producing solid materials from small molecules, and is considered to be a promising route to design nanosized electrode materials for LIBs [178]. It is because that the sol-gel method has a series of advantages over the traditional solid-state reaction, such as homogeneous mixing the reactants at the atomic or molecular level, low synthesis temperature, short heating time, small particle size on a nanometer scale and uniform particle distribution [179]. Sol-gel process is the conversion of a colloidal suspension (sol) into an integrated 3D network (gel) with pores of submicrometer dimensions and polymeric chains whose average length is greater than 1 μm [180]. Specifically, it involves several steps: precursor → hydrolysis → reactive monomer → condensation → sol gelation → gel → further treatment [179]. According to this synthetic procedure, various precursors (*e.g.*, V_2O_5 [181], and NH_4VO_3 [182] as vanadium sources), solvents (*e.g.*, deionized water [183], and 1,2-propylene glycol [184]), chelating agents (*e.g.*, citric acid [139, 145, 185-187], polyvinylpyrrolidone (PVP) [188], oxalic acid [189], glycine [190], and poly(vinyl alcohol) (PVA) [156],) have been used to assist sol-gel preparation of LVP cathode materials. Taking PVA as an example [156], 5 wt% PVA was added to an aqueous solution containing stoichiometric Li_2CO_3, $NH_4H_2PO_4$, and NH_4VO_3 under vigorous stirring, followed by evaporation at 120 ^oC to get a gel precursor. Then the precursor was heat treated at 750 ^oC for 4 h in N_2 atmosphere. PVA was employed here not only as a chelating reagent but also as a carbon source. The as-synthesized carbon coated LVP (LVP/C) displays a particle morphology with size of

200-500 nm (**Fig. 6B**), and shows a good cycling performance (*e.g.*, 100 mAh g^{-1} at 1 C rate between 3.0 and 4.3 V *vs.* Li/Li^+).

5.3. Hydrothermal method

Hydrothermal method with advantages of simplicity, homogeneous products, narrow particle-size distributions, morphology control, fast reaction kinetics, short processing times, phase purity, high crystallinity, low temperature post-calcination, low cost, *etc*., has been extensively studied over many decades for the synthesis of a variety of functional nanomaterials with specific sizes and shapes [191-195]. In the hydrothermal process, water is used as the main reaction medium with proper reactants placed in a Teflon-lined autoclave, which is then heated to a targeted temperature to accelerate the reaction. Generally, the temperature is higher than the boiling point of water (100 ^oC) to develop a high self-generated vapor pressure in a closed system. Nowadays, the hydrothermal process has become an important technique for the synthesis of various electrode materials for LIBs [192].

In 2008, Chang *et al*. [196] reported the preparation of flake-like LVP/C (1-3 μm) under hydrothermal reaction condition at 160 ^oC for 2 h, where $LiOH{\cdot}H_2O$, NH_4VO_3, and $NH_4H_2PO_4$ were used as starting materials in a molar ratio of 3 : 2 : 3. Besides, glucose was also used as the reducing agent and the carbon source for conductive coating. To increase the crystallinity, the hydrothermal product was further fired at 700 ^oC for 6 h under flowing Ar. The resulting LVP/C shows a discharge capacity of 142 mAh g^{-1} after 50 cycles between 3.0 and 4.8 V *vs.* Li/Li^+ at a rate of 1 C, whereas LVP/C particles (2-4 μm) prepared by the solid-state reaction only have 122 mAh g^{-1}. In 2010, Liu *et al*. [197] reported the hydrothermal synthesis of LVP nanorods at 180 ^oC for 24-36 h without subsequent calcination step. Li_2CO_3, V_2O_5, $HOOCCOOH{\cdot}2H_2O$ and H_3PO_4 were used as the starting materials. The obtained LVP nanorods have diameters of ~60 nm and lengths of around 0.5-1 μm, and display a superior rate capability (*e.g.*, 101.1 mAh g^{-1} at 10 C

between 3.0 and 4.6 V *vs.* Li/Li^+). Qiao *et al*. [198] investigated the effect of different synthetic routes on structure and electrochemical performance of LVP/C cathodes. It is found that the LVP/C synthesized by hydrothermal method shows smaller particle size, higher discharge capacity, better rate capability than those by solid-state reaction and sol-gel method. Even at a high charge/discharge rate of 10 C, the hydrothermal-derived LVP/C still can deliver a capacity of 106.6 mAh g^{-1} in the potential range of 3.0-4.8 V *vs.* Li/Li^+. Very recently, Duan *et al*. [199] synthesized LVP@C core-shell nanoparticles with sizes of 20-40 nm using a hydrothermal-assisted method (**Fig. 6C**). Ascorbic acid and polyethylene glycol 400 (PEG-400) were adopted as carbon sources and reductants. In the hydrothermal process, a partially carbonized layer was formed, which hindered the particle growth during the high-temperature calcination. The as-prepared LVP@C nanocomposite exhibits a remarkably high rate capability and long cyclability, delivering a discharge capacity of 138 mAh g^{-1} at 5 C within the voltage range of 3-4.8 V *vs.* Li/Li^+ and a capacity retention of 86% after 1000 cycles.

5.4. Spray pyrolysis

Spray pyrolysis is a powerful technique to continuously produce a wide variety of ceramic powders in a single-step for a short operative time [200]. Apart from its simplicity, spray pyrolysis technique has capability to produce high purity, chemically homogenous powders with fine size, non-agglomerate, and spherical morphology. The spray pyrolysis apparatus is mainly composed of a droplet generator, a quartz reactor and a powder collector [201]. In spray pyrolysis, precursor solution is initially carried into a heated tubular reactor through a carrier gas, where the solvent in the droplets is evaporated and solid particles are formed. Subsequently, the solid particles are treated in the high temperature zone of the reaction tube to form the crystallized phases. Depending on the process parameters such as

precursor solution, atomization of precursor solution, aerosol transport and decomposition of precursor, it is available to synthesize particles with well controlled morphology and composition.

Ko *et al*. [202] reported the ultrasonic spray pyrolysis synthesis of spherical LVP/C powders with sucrose as the carbon source. The precursor solution was prepared by dissolving stoichiometric amounts of lithium carbonate, vanadium oxide, and ammonium dihydrogen phosphate in a dilute nitric acid solution with the addition of sucrose. The reactor temperature was set at 1300 ^{o}C. The precursor powders obtained by spray pyrolysis have a spherical shape irrespective of the concentration of sucrose. After post-treatment at 700 ^{o}C for 3 h in 10% H_2/N_2 atmosphere, the spherical shape of precursors with sucrose is retained (*e.g.*, 0.1 M sucrose, **Fig. 6D**), whereas the spheres are collapsed with severe aggregation in the absent of sucrose. Later the same group synthesized nano-sized LVP/C composite powders by combination of spray pyrolysis and milling process [203]. Citric acid and ethylenediaminetetraacetic acid (EDTA) were used as chelating agents to control the morphologies of the LVP precursor powders. Hollow, thin-walled precursor spheres are obtained at the optimized concentrations of citric acid and EDTA (0.1 M), and maintained after the post-treatment. Moreover, the hollow structures are easily pulverized into fine nanoparticles by simple milling process. The as-synthesized nano-sized LVP/C exhibits higher discharge capacity, better cycling stability and rate performance than the bare LVP.

5.5. Freeze-drying method

Recently, freeze-drying method has also been used for the preparation of LIB cathodes such as $LiNi_{0.5}Mn_{0.5}O_2$ [204], $Li_{1.131}Mn_{0.504}Ni_{0.243}Co_{0.122}O_2$ [205], and LFP [206]. This cryochemical route is simple, and can provide the opportunity to obtain the products with high homogeneity and fine particle size. In 2012, Wang *et al*. [207] applied the freeze-drying method to synthesize the homogeneous LVP/C. In a typical synthesis procedure, a colloid sol containing

NH_4VO_3, $LiOH·H_2O$, H_3PO_4, and citric acid was initially poured drop-by-drop into liquid nitrogen, followed by another vacuum drying process at -40 ^oC to remove the solid solvent completely. $Li_3V_2(PO_4)_3$/C was finally obtained by sintering at high temperature in N_2 atmosphere. As indicated by the scanning electron microscope (SEM) image (**Fig. 6E**), the prepared LVP/C has particle size of around 1-2 μm, and every particle is enwrapped by a homogeneously transparent carbon layer. In addition, a porous structure is also detected (inset in **Fig. 6E**), which is most probably due to the fast removal of the solid solvent during the precursor preparation. This LVP/C cathode shows good high rate performance (*e.g.*, delivering 85 mAh g^{-1} at 30 C rate) and cycling stability (*e.g.*, no capacity fading at 10 C after 300 cycles) in the potential window of 3.0-4.3 V *vs.* Li/Li^+. Another freeze-drying work on the LVP was carried out by Qiao *et al*. [208]. The synthesis procedure is similar, and polystyrene (PS) spheres were used as the carbon source. The as-prepared LVP/C shows a uniform particle size distribution and the particle size is less than 300 nm. The electrochemical property test indicates that the LVP/C has high rate capability and excellent cycling stability, *e.g.*, delivering an initial discharge capacity of 93 mAh g^{-1} at a high rate of 30 C, and sustaining at 61 mAh g^{-1} after 500 cycles.

5.6. Electrospinning

Electrospinning has been widely used to produce continuous nanofibers of various organic, inorganic, and hybrid materials with controlled diameter, morphology and surface topology [209-211]. Electrospinning is a top-down approach with the advantages of simple, versatile, cost-effective, high yield, and high degree of reproducibility of the obtained materials [209]. The principle of electrospinning is based on the application of an electric field between the syringe (spinneret) and collector. When the applied electric field reaches a critical value, the electrostatic repulsions among the charges on the surface of the drop overcome the surface tension, and a jet is drawn from the spinneret under a

constant flow rate. This facile method has been successfully applied to produce a series of nanofiber electrode materials for LIBs [212-214]. In the case of LVP, a pioneer work regarding the electrospinning method was carried out by Chen *et al*. [215] using a homogeneous viscous aqueous solution containing raw materials of NH_4VO_3, $NH_4H_2PO_4$, $CH_3COOLi{\cdot}2H_2O$, PVP, and citric acid. The precursor nanofibers were then calcined at 800 ^oC for 4 h in Ar atmosphere. The obtained LVP/C fibers have diameters of 90-220 nm, and lengths of up to 5-20 μm (**Fig. 6F**). The specific surface area is measured to be as large as 160.75 $m^2\ g^{-1}$, which yields high contact area with the electrolyte, resulting in the improved electrochemical performance, *e.g.*, delivering a high discharge capacity of 190 mAh g^{-1} at 0.1 C between 3.0 and 4.8 V *vs.* Li/Li^+, and 132 mAh g^{-1} even at a high rate of 20 C.

5.7. Electrostatic spray deposition

Electrostatic spray deposition (ESD) has recently attracted much attention as a promising technique for the fabrication of inorganic thin films, especially for LIB electrode materials [216-219]. It has shown many advantages over some conventional deposition techniques (*e.g.*, sputtering, and chemical vapor deposition), such as a simple set-up, non-vacuum, high deposition efficiency, and easy control of the surface morphology of the deposited layers (*e.g.*, sponge-like, dense, fractal-like, and cross-linked porous structures, *etc*.). The ESD is based on applying a high direct current (DC) voltage between the nozzle and the grounded substrate to atomize the precursor solution into the aerosol. Specifically, the whole process involves five steps: (1) spray production; (2) droplet transportation, evaporation, and disruption; (3) preferential landing of droplets on the substrate; (4) discharge, spreading and penetration of solution droplets on the surface; and (5) decomposition, reaction and surface diffusion of the solutes [216].

In 2009, Wang *et al*. [220] reported the fabrication of a LVP/C film *via* the ESD technique. The precursor solution was prepared by dissolving the raw materials of NH_4VO_3, $LiNO_3{\cdot}H_2O$, H_3PO_4, and glucose in a mixed solvent

containing deionized water, ethanol, and 1,2-propylene glycol. A flat graphite sheet was used as the substrate and heated at 240 ^{o}C, and the applied DC voltage was 12.5 kV. The deposited film was finally thermal treated at 700 ^{o}C for 8 h in Ar atmosphere. Interestingly, the obtained LVP/C film exhibits a walnut-kernel-like morphology with size of around 10 μm (**Fig. 6G**). The transmission electron microscopy (TEM) analysis reveals that the film is comprised of many small LVP crystals (about 50 nm) distributed in a continuous carbon matrix. In the voltage range of 3.0-4.3 V *vs.* Li/Li^{+}, such a nanostructured LVP/C thin film shows stable capacity retention and excellent rate capability, *e.g.*, delivering 80 mAh g^{-1} at 24 C.

5.8. Other methods

In addition to the above-mentioned classic preparation methods, some other approaches have also been demonstrated to produce LVP cathode materials. One of them is the rheological phase reaction method [221-223]. Actually, it is a liquid-solid phase reaction in which the solid particles and liquid substances are uniformly distributed. Chang *et al*. [221] were the first to fabricate LVP/C using this method. Stoichiometric Li_2CO_3, V_2O_5, and $NH_4H_2PO_4$ were initially mixed by grinding, and then appropriate amount of polyethyleneglycol 300 (PEG-300) and water were added to get a rheological body. In this rheological system, solid-state starting materials are coated efficiently by PEG-300 fluid, resulting in a high-quality carbon coating during the calcination process (**Fig. 6H**). The electrochemical properties of LVP/C in terms of the capacity and cycling stability obtained by rheological phase reaction are much better than that synthesized by the conventional solid-state reaction. An *in situ* polymerization method was also introduced to synthesize high performance LVP/C using acrylamide as monomer, $(NH_4)_2S_2O_8$ as initiator, N,N'-methylenebisacrylamide (MBA) as cross-linking agent [159]. After carbonization, a 3D carbon network is obtained, which provides conductive pathways in favor of electron transport and the kinetic extraction/insertion of Li

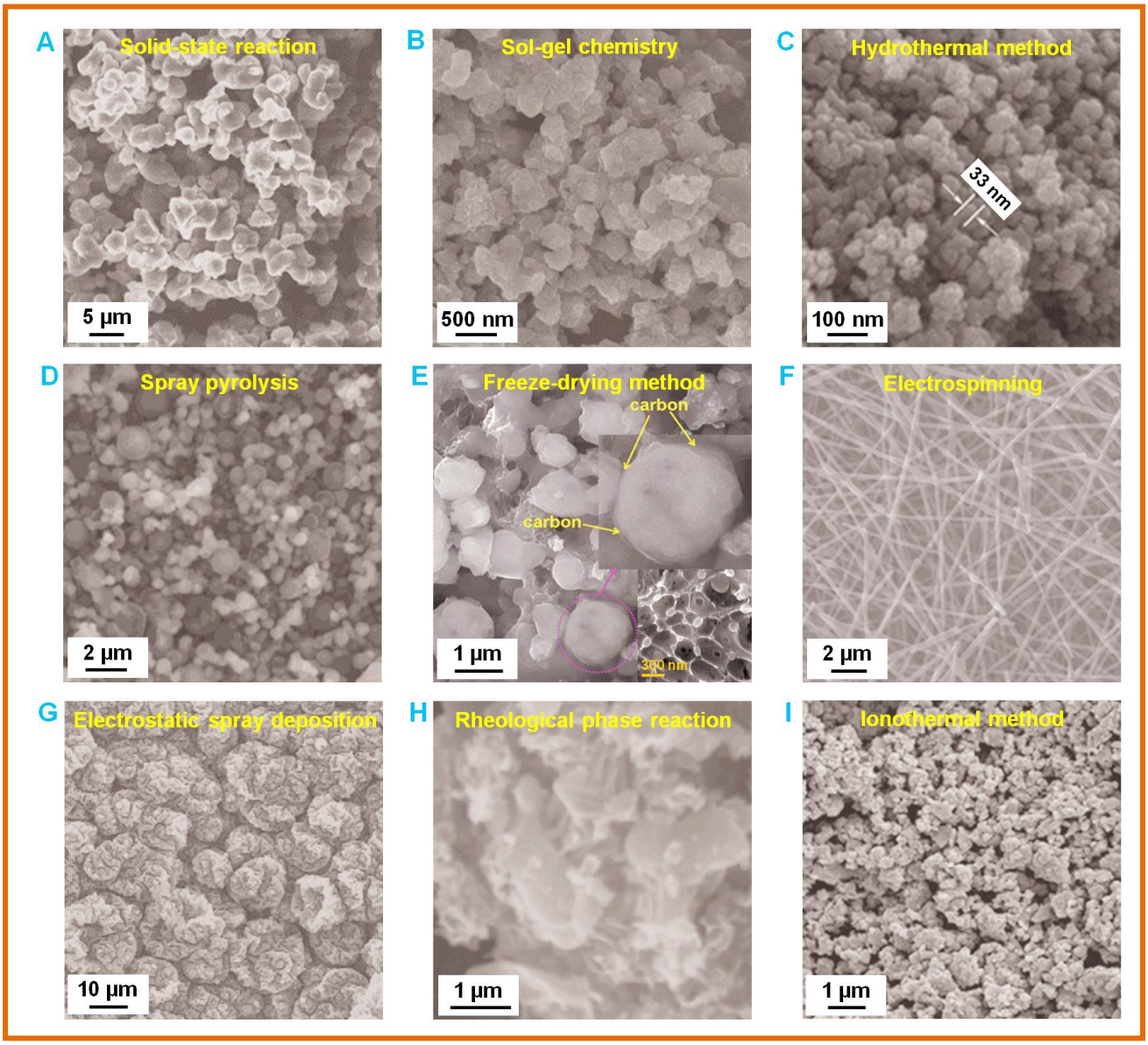

Fig. 6 The morphology of LVP cathode materials prepared by different methods. (A) Solid-state reaction. Reproduced with permission from [123]. (B) Sol-gel chemistry. Reproduced with permission from [156]. (C) Hydrothermal method. Reproduced with permission from [199]. (D) Spray pyrolysis. Reproduced with permission from [202]. (E) Freeze-drying method. Reproduced with permission from [207]. (F) Electrospinning. Reproduced with permission from [215]. (G) Electrostatic spray deposition. Reproduced with permission from [220]. (H) Rheological phase reaction. Reproduced with permission from [221]. (I) Ionothermal method. Reproduced with permission from [226].

ions. Nathiya *et al*. [224] explored a combustion reaction method to produce nanocrystalline LVP/C composite (around 50 nm) using corn (*i.e.*, a cheap and commonly available polysaccharide) as fuel, which decomposed (< 200 ^{o}C) into a finely cooked fluffy mass to hinder the particle growth during the high-temperature calcination. Nagamine *et al*. [225] reported a fast synthesis of LVP/C crystals *via* a glass-ceramic processing. A glass with the composition of $37.5Li_2O$-$25V_2O_5$-$37.5P_2O_5$ (mol%, mole percent) was initially prepared by a conventional melt-quenching method and then crystallized with 10 wt% glucose in 7%H_2/Ar atmosphere at 700 ^{o}C to form LVP/C particles. Li *et al*. [226] developed an ionothermal method to synthesize nanostructured LVP/C cathode materials using three kinds of imidazolium-based ionic liquids (*i.e.*, 1-ethyl-3-methylimadozolium tetrafluoroborate ([emim][BF_4]), 1-ethyl-3-methylimadozolium trifluoromethanesulfonate ([emim][OTf]), and 1-ethyl-3-methylimadozolium acetate ([emim][OAc])) as both reaction mediums and structure-directing agents. It is found that the LVP/C sample prepared from [emim][OAc] presents smaller particle size (0.2-1 μm) and more uniform particle size distribution (**Fig. 6I**), and thus exhibits higher reversible capacities under various current rates.

6. Approaches to improve the electrochemical properties

6.1. Carbon coating

Coating of the LVP particle surface with amorphous carbon is the most common way to enhance its electronic conductivity so that the active materials can be largely utilized at high current rates [167, 227-230]. Carbon coating can also alleviate the growing up and aggregation of LVP particles during the high-temperature calcination. Additionally, carbon can act as a reducing agent to reduce V^{5+} to V^{3+} and thus simplify the atmosphere requirement in the synthesis [137]. The carbon coating is usually realized by introducing carbon sources in the starting materials, including carbon black [169], high area carbon [170], Ketjenblack carbon [163], carbon nanoflakes [231], and organic precursors such as

citric acid [186, 232-234], maleic acid [235], ascorbic acid [198, 236], humic acid [166], stearic acid [157], sucrose [237-239], glucose [162, 167], maltose [189], crystal sugar [230, 240], starch [241], chitosan [242], EDTA [222], PS spheres [208, 243], PVP [188], *β*-cyclodextrin [182], PVA [244-246], carboxy methyl cellulose (CMC) [247], glycine [190], phenolic resin [123], PEG-400 [248], PEG-10,000 [249], poly(vinylidene difluoride) (PVDF) [137], 1,4-dihydroxy-2-butyne [250], and Baker's yeast cells [251], *etc*. For the organic precursors, they can be converted into electronically conductive carbon through pyrolysis processes at high temperatures under inert atmosphere.

A seven-order-of-magnitude increase in the electronic conductivity is obtained by adding PEG-10,000 to produce carbon coated on LVP raw materials through a simple solid-state reaction [249]. The TEM images (**Fig. 7**) clearly depicts that a carbon layer (*ca*. 30-40 nm) is uniformly coated on LVP particle surface, and LVP particles are connected very well through the carbon network. The as-prepared LVP/C composite not only achieves almost theoretical capacity but also shows good rate capability and excellent cycling stability in the voltage range of 3.0-4.3 V *vs.* Li/Li^+. Actually, the effects of carbon coating on the electrochemical properties of LVP are mainly dependent on its quality, including the carbon content, the degree of graphitization, the morphology and the distribution of the carbon on LVP surface. Although the conductivity of LVP can be significantly improved by carbon coating, excess carbon may lead to the obstruction of lithium ion diffusion, and will seriously decrease the tap density. Hence, it is necessary to optimize the carbon content. Rui *et al*. [189] designed a maltose-assisted sol-gel method to synthesize LVP/C composites, and the carbon content was controlled by the amount of maltose. With increasing the maltose amount, four LVP/C samples with different carbon contents of 5.7, 9.6, 11.6 and 15.3 wt% are obtained. The electrochemical results show that the sample with 11.6 wt% carbon content exhibits the lowest charge-transfer resistance and the best electrochemical properties, especially for the rate capability, *e.g.*, the capacity decreasing by only 7.2% from 125 mAh g^{-1} at 0.5 C to 116 mAh g^{-1}

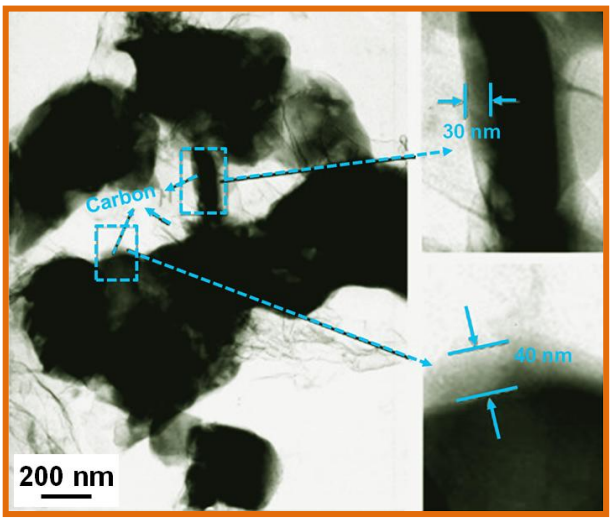

Fig. 7 TEM images showing a carbon layer (*ca*. 30-40 nm) uniformly coated on LVP particle surface, and good connection of LVP particles through the carbon network. Reproduced with permission from [249].

at 5 C between 3.0 and 4.3 V *vs.* Li/Li^+ (**Fig. 8A**). Jiang *et al*. [239] reported that the optimal carbon content in LVP/C is 7.7 wt% on the base of a carbothermal reduction method using sucrose as the carbon source.

Research on carbon coating has also focused on degree of graphitization (*i.e.*, the sp^2/sp^3 ratio). Graphite carbon (sp^2-coordinated) is more conductive, and allows faster Li^+ diffusion than disordered carbon (sp^3-coordinated) [252]. In general, the amount of graphite carbon in the coating can be detected from the band-intensity ratio of graphite (I_G) and disordered carbon (I_D) in the Raman spectroscopy. The I_G/I_D ratio is closely related to the carbon source and the sintering temperature, and much effort has been made to obtain high-quality carbon coatings. Recently, a I_G/I_D ratio of 1.15 is obtained by an *in-situ* carbonization of PEG-10,000 at 850 ^oC [249]. Later a higher quality carbon coating (I_G/I_D = 1.56) is achieved by a carbothermal reduction method (850 ^oC) using PVA as the carbon source [246]. The as-prepared LVP/C composite presents a long-term cyclability, retaining more than 90% of initial capacity after 2000

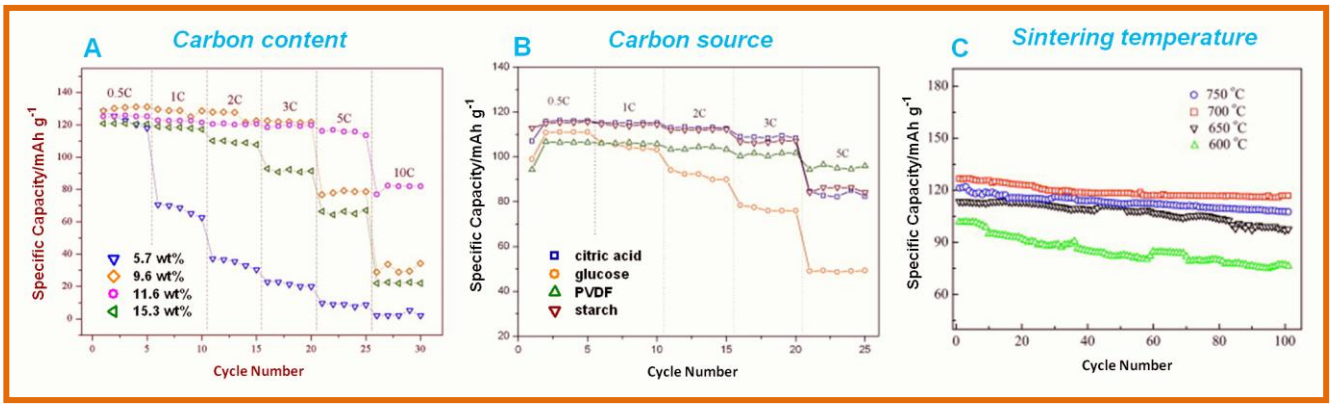

Fig. 8 The effects of different carbon content (A), carbon sources (B), and sintering temperatures (C) on the electrochemical properties of carbon coated LVP. (A-C) were reproduced with permission from [189], [137], and [157], respectively.

cycles at a high rate of 5 C between 3.0 and 4.2 V *vs.* Li/Li^+. In this way, high-quality carbon coating can reduce the consumption of conductive carbon, and thus increase the tap density.

In addition to the degree of graphitization, different carbon sources and sintering temperatures have different effects on the morphology and distribution of carbon deposited on the surface of LVP particles, and the crystallinity of LVP, leading to different electrochemical properties of LVP. Rui *et al*. [137] investigated the influence of four selected carbon sources (*i.e.*, citric acid, glucose, PVDF and starch) on the electrochemical performance of LVP/C composites. With keeping the same molar ratio of carbon atom to LVP, the residual carbon is determined to be 1.3, 13.3, 12.7, and 10.5 wt% in LVP/C composites that derived from carbon sources of citric acid, glucose, PVDF and starch, respectively. The lowest carbon content for citric acid is attributed to the existence of carboxyl, which could decompose to CO_2 gas instead of contributing to residual carbon during the heating process. The morphology analysis indicates that the LVP/C prepared from PVDF has relatively homogeneous coating of carbon, and nano-sized particles. Of all four samples,

PVDF-derived LVP/C exhibits the best rate capability, *e.g.*, possessing a capacity of 95 mAh g^{-1} even at a high rate of 5 C in the voltage region of 3.0-4.3 V *vs.* Li/Li^+ (**Fig. 8B**). One of work on sintering temperatures was carried out by Qiao *et al*. [157]. They LVP/C composites were synthesized by a carbothermal reduction method under sintering temperatures of 600, 650, 700 and 750 ^oC using stearic acid as the carbon source. It is found that the LVP phase is not well crystallized at a low temperature of 600 ^oC, and the particle size becomes larger at higher temperature of 750 ^oC. TEM study shows that LVP particles prepared at 700 ^oC is coated with a uniform carbon layer (a thickness of ~13 nm), which is believed to improve the electronic conductivity and thus results in the enhanced electrochemical properties. For example, it has 7.8% capacity loss of the initial capacity between 3.0 and 4.3 V *vs.* Li/Li^+ at 1 C, while regarding to the LVP/C samples synthesized at 600, 650 and 750 ^oC, the values are as high as 24.9%, 14.0%, and 11.3%, respectively (**Fig. 8C**).

More details about the effect of the carbon coating on the electrochemical performance of LVP cathodes are summarized in **Table 1**.

Table 1 The effect of carbon coating on the electrochemical performance of LVP cathodes

Carbon				Preparation method	Electrochemical performance	References
Sources	Content	Thickness	Structure (I_G/I_D)			
Glucose	~4.8 wt%	~10 nm	—	Sol-gel and hydrothermal	In 3.0-4.5 V, showing an initial capacity of 127.8 mAh g^{-1} with a capacity retention of 98.5% after 50 cycles at ~0.2 C	[162]
PVA-2000	3.1 wt%	~6 nm	1.02	Sol-gel	In 3.0-4.3 V, reversible capacity of 100 mAh g^{-1} at 1 C	[156]
PS	0.39-2.28 wt%	~1-30 nm	—	Carbothermal reduction (CTR)	In 3.0-4.3 V, 132.7 mAh g^{-1} at 0.1 C	[243]
Stearic acid	2.67-3.1 wt%	~1-13 nm	—	CTR	In 3.0-4.8 V, 185.9, 140.9, and 112.1 mAh g^{-1} at 0.1, 5, and 15 C, respectively	[157]
Oleic acid	~2 wt%	—	—	CTR	In 3.0-4.3 V, 131 mAh g^{-1} at 1 C	[253]
Sucrose	7.5 wt%	—	—	Spray pyrolysis	In 3.0-4.8 V, 138 mAh g^{-1} (1^{st} cycle) at 0.1C	[202]
Ascorbic acid	1.72 wt%	~6 nm	—	Hydrothermal	In 3.0-4.8 V, 106.6 mAh g^{-1} at 10 C	[198]
Sucrose	~5 wt%	~5 nm	—	Hydrothermal	In 3.0-4.8 V, 145 mAh g^{-1} (1^{st} cycle) at 0.1C	[254]
1,4-dihydroxy-2-butyne	2.62 wt%	—	1.15	Hydrothermal	In 3.0-4.8 V, 183.8, 160.9, and 121.5 mAh g^{-1} at 0.2, 1, and 15 C, respectively	[250]
Glycine	8 wt%	~8 nm	—	Sol-gel	In 3.0-4.3 V, 125.4, and 99.5 mAh g^{-1} at 1, and 20 C, respectively	[190]
Citric acid	3.98 wt%	10-20 nm	—	Freeze-drying	In 3.0-4.3 V, 110.8, 97.9, and 85 mAh g^{-1} at 5, 10, and 30 C, respectively	[207]
Baker's yeast cell	16.4 wt%	—	—	Biomimetic approach	In 3.0-4.3 V, 126.7, and 100.5 mAh g^{-1} at 0.2, and 5 C, respectively	[251]
PVA-124	4.63 wt%	~10 nm	1.15	CTR	In 3.0-4.8 V, 187.6 mAh g^{-1} at 0.1 C and 140 mAh g^{-1} at 10 C	[244]
Citric acid	1.57-4.56 wt%	~2-3 nm	—	Sol-gel	In 3.0-4.3 V, 117.6, and 83.6 mAh g^{-1} during the 150^{th} cycle at 10 and 20 C, respectively	[186]
Starch	3.45 wt%	—	—	CTR	In 3.0-4.3 V, 130 mAh g^{-1} at 0.1 C and 91.5 mAh g^{-1} at 2 C	[241]
Citric acid	4.1 wt%	~2.5 nm	—	Spray-drying	In 2.5-4.5 V, 161.3 mAh g^{-1} at 0.1 C and 111.64 mAh g^{-1} at 10 C	[232]
Glycine and β-cyclodextrin	7.5 wt%	~5 nm	—	Sol-gel	In 3.0-4.3 V, 74.5 mAh g^{-1} with 90.8% capacity retention after 250 cycles at 50 C	[182]
PVP	0.98-3.48 wt%	~12 nm	—	Sol-gel	In 3.0-4.3 V, 127.2, 115.1, and 81.8 mAh g^{-1} at 1, 10, and 20 C, respectively	[188]
Maleic acid	3.3-5.8 wt%	~5 nm	1.21	Sol-gel	In 3.0-4.8 V, 179.8, and 154.6 mAh g^{-1} at 0.1, and 0.5 C, respectively	[235]
PS	4.21 wt%	~9 nm	1.16	Freeze-drying	In 3.0-4.3 V, 105.6 and 93.3 mAh g^{-1} at 15	[208]

					and 30 C, respectively	
Chitosan	9.8 wt%	~5 nm	—	CTR	In 3.0-4.3 V, 106.9 mAh g^{-1} at 20 C	[242]
Corn	12 wt%	~6 nm	—	Combustion	In 3.0-4.8 V, 174 mAh g^{-1} (1^{st} cycle) at 0.1 C	[224]
EDTA	10 wt%	~60 nm	—	Rheological phase	In 3.0-4.3 V, 129.1 mAh g^{-1} (1^{st} cycle) at 0.1 C and 108 mAh g^{-1} (100^{th} cycle) at 2 C	[222]
Polyacrylamide	3.3-7.2 wt%	—	—	Polymerization	In 3.0-4.3 V, 119.02 mAh g^{-1} at 10 C	[159]
CMC	~3.3 wt%			Spray-drying	In 3.0-4.8 V, 172.3 mAh g^{-1} (1^{st} cycle) at 0.1 C and 106.2 mAh g^{-1} at 2 C	[247]

6.2. Graphene modification

Graphene, a monolayer of sp^2-bonded carbon atoms arranged in six-membered rings, has become one of the most exciting topics of research in the last several years due to its extraordinary electrical/thermal conductivities, ultrahigh specific surface area, good mechanical strength and chemical stability [255-257]. On the basis of these advantages, incorporation of graphene with electrode materials including anodes and cathodes has been successfully developed and was reported to have superior electrochemical performance for LIBs [258-261]. Of course, graphene can also serve as the conducting support material to enhance the capacity delivery and cycle performance of LVP batteries [141, 262-269].

In 2011, Liu *et al*. [262] firstly reported the preparation of LVP/graphene nanocomposite through a solution-based process combined with high temperature reaction. Based on these two steps, well-crystallized LVP nanoparticles with sizes of 50-500 nm are adhered to the surface of the graphene layer and/or enwrapped into the graphene sheets. Minor amount of graphene (less than 1.14 wt%) in LVP/graphene composite results in a large improvement of the rate performance and cycling stability. For example, a discharge capacity of 82 mAh g^{-1} is pronounced at a very high current rate of 50 C between 3.0 and 4.3 V *vs.* Li/Li^+. Lately, our group introduced a nanoporous carbon matrix in addition to

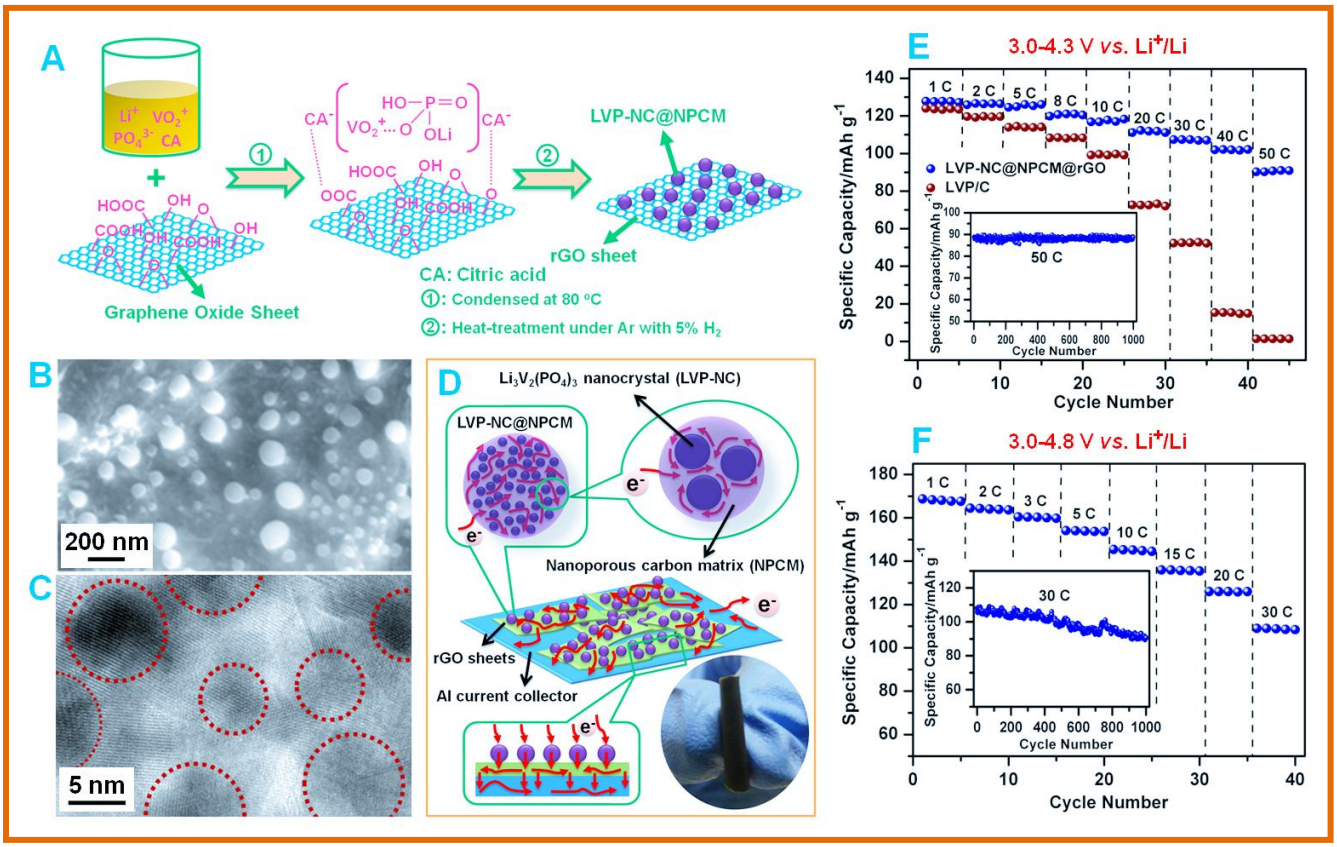

Fig. 9 (A) Schematic illustration of the formation mechanism of LVP-NC@NPCM@rGO. (B) SEM image. (C) HRTEM image. (D) Electron transfer pathways throughout the whole binder-free LVP-NC@NPCM@rGO electrode and corresponding optical image (inset). (E) Comparison of discharge capacities of binder-free LVP-NC@NPCM@rGO and normal LVP/C electrodes at various current rates between 3.0 and 4.3 V *vs.* Li/Li^+. Inset: cycling performance of LVP-NC@NPCM@rGO electrode at 50 C. (F) Rate capability of binder-free LVP-NC@ NPCM@rGO electrode in a wider voltage window (3.0-4.8 V *vs.* Li/Li^+) and corresponding cycling performance at 30 C (inset). Reproduced with permission from [267].

the graphene to further improve the electron transportation [267]. By using a sol-gel-based route, LVP nanocrystals embedded in a nanoporous carbon matrix attached onto reduced graphene oxide (rGO) sheets (abbreviated as

LVP-NC@NPCM@rGO) are obtained. Here, it is worth to mention that the graphene sheet obtained by the chemical/thermal reduction method is also known as rGO. The synthetic procedure and mechanism is schematically illustrated in **Fig. 9A**. The presence of graphene oxide sheets not only acts as the heterogeneous nucleation site to facilitate the growth of nanograins of LVP, but also helps to separate the LVP grains and prevent the coarsening of LVP particles during the heat treatment process. SEM image (**Fig. 9B**) shows that quasi-spherical particles with a size of 20-80 nm are uniformly anchored onto the surface of rGO nanosheets. The high-resolution (HR) TEM image (**Fig. 9C**) of a single nanoparticle reveals that it consists of LVP nanograins with sizes in the range of 5-8 nm embedded in an amorphous nanoporous carbon matrix. The mesopores carbon feature is further confirmed by the Barrett-Joyner-Halenda (BJH) analysis with an average pore size of 3.3 nm. Such hierarchical structure including highly conductive rGO sheets and carbon matrix ensures the fast charge transfer within the whole electrode and to the current collector (**Fig. 9D**). Additionally, the nanoporous carbon can act as an electrolyte container to allow fast Li^+ migration to each LVP nanoparticle, and also provides an elastic buffer to maintain structural integrity during repeated charge-discharge processes. Furthermore, the flexibility of rGO sheets is benefit to fabricate the binder-free cathode (inset in **Fig. 9D**), which can further improve the electrical conductivity and electrolyte permeation in the electrode. Combining with short Li^+ diffusion distance for ultrafine LVP nanocrystals (5-8 nm), the LVP-NC@NPCM@rGO cathode exhibits excellent lithium storage performance, especially at high current densities. In the voltage region of 3.0-4.3 *vs.* Li/Li^+ (**Fig. 9E**), even at a very high current rate of 50 C, it can still deliver a high capacity of 90 mAh g^{-1}, and maintains at 88 mAh g^{-1} after 1000 cycles. While the LVP/C electrode prepared in the absent of rGO sheets only shows low discharge capacities of 52 and 15 mAh g^{-1} at 30 and 40 C, respectively, and even cannot be discharged at a high rate of 50 C. In the voltage region of 3.0-4.8 *vs.* Li/Li^+ (**Fig. 9F**), the LVP-NC@NPCM@rGO cathode delivers discharge capacities of 145, 126 and 109 mAh g^{-1} at current rates of 10, 20, and 30 C, respectively. Also, a superior

cycling performance at 30 C is achieved in such wider voltage window (inset in **Fig. 9F**), showing a discharge capacity of 91 mAh g^{-1} during the 1000^{th} cycle.

6.3. Other conductive coatings and additives

Alternatives to carbon coating and LVP/graphene hybrids include some metal, metal oxide, and glassy lithium phosphate coatings, as well as some conductive additives, which can also improve considerably the kinetics of LVP without altering the crystal structure [147, 270-276]. In 2010, Zhang *et al*. [270] made LVP/(Ag + C) composites through carbothermal reduction method using polypropylene as both reduction agent and carbon source followed by chemical plating of Ag on LVP/C. From the HRTEM images in **Fig. 10A**, it is found that Ag nanoparticles with diameter of about 15 nm are loaded on the LVP/C particles. Electrochemical impedance spectroscopy (EIS) measurements show that, as compared to pure LVP and LVP/C cathodes, the charge transfer resistance of carbon and silver co-modified LVP/(Ag + C) cathode is significantly decreased, leading to its highest discharge capacity (172 mAh g^{-1}) at 0.1 C between 3.0 and 4.8 V *vs.* Li/Li^+ (**Fig. 10B**).

Surface modifications of olivine-type phosphate materials by coating nonelectroactive metal oxides have been proved to be an effective method in improving the cathode performance [277]. In the case of lithium vanadium phosphate, Zhai *et al*. [271] modified LVP/C with a coating of MgO nanolayer (*ca*. 2 nm). Electrochemical measurements in terms of galvanostatic charge/discharge, EIS and cyclic voltammetry clearly show that MgO nanocoating stabilizes the structure of LVP cathode and decreases the interface charge transfer resistance, and thus enhances the reversibility of electrode reaction. Another work was SiO_2-modified LVP/C cathode [272]. $Li_3V_2(PO_4)_3$/C powders coated with various amounts of SiO_2 were synthesized by using tetraethyoxysilane (TEOS) as the silica source with the concentration of TEOS being 1, 2, and 3 wt% of LVP/C (abbreviated as LVP/C-1Si, LVP/C-2Si, and

LVP/C-3Si samples), respectively. The successful SiO_2 coating was confirmed by the analysis of X-ray diffraction (XRD), X-ray photoelectron spectroscopy (XPS), and TEM. HRTEM image (**Fig. 10C**) of LVP/C-2Si indicates that the LVP particles are wrapped with a mixed amorphous carbon and SiO_2 layer with a thickness of 3-5 nm. Electrochemical tests reveal that LVP/C-2Si electrode shows remarkably improved electrochemical performance, especially at high C-rates. For example, LVP/C-2Si electrode delivers discharge capacities of 136 and 125 mAh g^{-1} at 2 and 5 C between 3.0 and 4.8 V *vs.* Li/Li^+ (**Fig. 10D**), respectively, which are higher than those of pristine LVP/C electrode (*i.e.*, 115 mAh g^{-1} at 2 C and 108 mAh g^{-1} at 5 C). It is believed to result from the alleviated vanadium dissolution, enhanced structural stability, and decreased charge-transfer resistance of the LVP/C cathode after SiO_2 modification. Besides metal oxides, glassy lithium phosphates are well known to be good, stable Li^+ conductor, and have been applied to build Li-ion transportation pathways in LFP [278] and $LiNi_{0.5}Mn_{1.5}O_4$ [279] cathodes. Regarding to LVP, Xun *et al*. [273] prepared $Li_4P_2O_7$ and Li_3PO_4 glass co-coated LVP (abbreviated as G-LVPO) from a non-stoichiometric set of precursors. The LVP phase is well crystallized at 900 ^oC, and a thin layer (<5 nm) of $Li_4P_2O_7$ and Li_3PO_4 coated on LVP is observed by TEM (**Fig. 10E**). The amorphous $Li_4P_2O_7$ and Li_3PO_4 coating provides a fast Li^+ ion transport pathway to the primary particles located in the interior of the secondary particles, as well as reduces the rate of side reactions, leading to better rate and cycling performance than those of bare LVP. For example, G-LVPO (capacity retention: 96.4%) demonstrates more stable cycling ability than bare LVP (capacity retention: 84.8%) at 1 C between 3.0 and 4.3 V *vs.* Li/Li^+ (**Fig. 10F**).

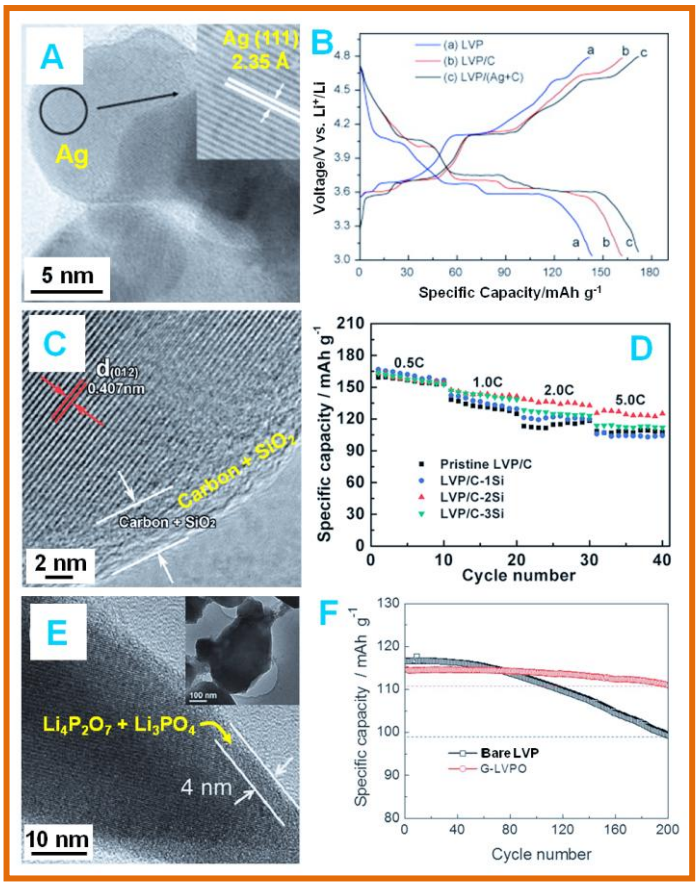

Fig. 10 (A) HRTEM images of LVP/(Ag + C), and (B) the first charge/discharge curves of LVP, LVP/C, and LVP/(Ag + C) electrodes at 0.1 C. Reproduced with permission from [270]. (C) TEM image of LVP/C-2Si, and (D) rate capability of pristine LVP/C, LVP/C-1Si, LVP/C-2Si, and LVP/C-3Si electrodes. Reproduced with permission from [272]. (E) TEM image of G-LVPO synthesized at 900 ^{o}C, and (F) cycling performance of bare LVP and G-LVPO at 1 C. Reproduced with permission from [273].

Introducing lithium metal oxide additives, such as $Li_4Ti_5O_{12}$ (LTO) [274], and LCO [275], is another effective way to improve the rate capability and capacity of LVP. Wang *et al*. [274] adopted a sol-gel method to prepare LVP/LTO/C composites. In the range of 3.0-4.3 V *vs.* Li/Li^+, such cathode exhibits excellent rate capability and cyclic performance, *e.g.*, reaching 75.5 mAh g^{-1} at discharge rate of 50 C (charge rate: 25 C), which are attributed to the existence of the

carbon with high electronic conductivity and LTO with high lithium ion diffusion coefficient (10^{-6} cm^2 s^{-1} [280]). Lately, they used electroactive LCO material as an additive to improve the electrochemical performance of LVP/C electrode.

6.4. Doping

Ion-doping is an efficient method to improve the intrinsic electronic conductivity and Li-ion diffusion. The positive effects of ion-doping on the capacity delivery, cycle life, and rate capability of LVP have been extensively demonstrated by different research groups [281-283]. Many supervalent cations, including Co^{2+} [284], Mn^{2+} [285], Ni^{2+} [286], Mg^{2+} [287], Ca^{2+} [254], Fe^{3+} [146], Cr^{3+} [161], Al^{3+} [288], Ce^{3+} [289], Sc^{3+} [254], Sn^{4+} [177], and Mo^{6+} [290], *etc.*, have been employed as dopants in the LVP system. Even multi-element doping [291-293] and anion doping [294] were also carried out.

It is known that the 3D framework of LVP is isotypic with its Ti, Fe, Cr, Al and Sc analogues [117, 126], which provides the opportunity to partly substitute vanadium with other metal ions. Doping with supervalent cations in LVP was first reported by Ren *et al*. [146] in 2006 using the dopant of Fe^{3+} as an useful method to improve the bulk conductivity and structural stability. The optimal Fe-doping content x is 0.02-0.04 in $Li_3V_{2-x}Fe_x(PO_4)_3$ system. It is found that the cell parameters of LVP decrease after incorporation of Fe^{3+} ions. The electrochemical tests reveal that the $Li_3V_{1.98}Fe_{0.02}(PO_4)_3$/C (1 wt%) shows the best charge/discharge cyclic stability from 177 mAh g^{-1} in the 1st cycle to 126 mAh g^{-1} in the 80th cycle (capacity retention: 71%) at C/5 rate in the range of 3.0-4.9 V *vs.* Li/Li^+, whereas the undoped LVP/C (1 wt%) only has a capacity retention of 58% (**Fig. 11A**). Later on, great effort has been devoted to further improve the capacity retention and rate capability of LVP by substitution of V^{3+} with a series of other supervalent metal ions (*e.g.*, Co^{2+}, Mg^{2+}, and Al^{3+}). Among them, Cr^{3+}-doped $Li_3V_{1.9}Cr_{0.1}(PO_4)_3$/C (6.5 wt%) compound shows promising results [161]. The Rietveld refinement of XRD patterns indicates that monoclinic single-phase $Li_3V_{2-x}Cr_x(PO_4)_3$/C (x =

0.05, 0.1, 0.2, 0.5, and 1) are obtained, and the lattice constants of *a*, *b*, *c*, and unit cell volume are also decreased with increasing Cr^{3+} content due to the difference of ionic radius of Cr^{3+} (0.64 Å) and V^{3+} (0.74 Å). Four-point probe measurements show that the electronic conductivity is increased by 10 times after doping. In the voltage region of 3.0-4.8 V *vs.* Li/Li^+, although the initial capacity is slightly decreased for Cr^{3+}-doped cathodes, cycling stability and high-C-rate performance are significantly enhanced when the Cr^{3+} content *x* is no more than 0.1. At various charge-discharge rates (**Fig. 11B**), $Li_3V_{1.9}Cr_{0.1}(PO_4)_3$/C exhibits the best capacity behavior (*e.g.*, ~115 mAh g^{-1} at 5 C). Doping individual bivalent (*e.g.*, Mg^{2+}) or tetravalent (*e.g.*, Sn^{4+}) cations at the V sites has the problem of charge imbalance, which may lead to the impurity in the product [285]. As a result, a codoping strategy is proposed. For example, Deng *et al*. [291] investigated the effect of Ti^{4+} and Mg^{2+} codoping on the structural and electrochemical properties of LVP. The as-synthesized $Li_3V_{2-2x}Ti_xMg_x(PO_4)_3$ (x = 0, 0.05, 0.1, 0.2, and 0.25) samples are found to be single-phase (monoclinic symmetry) with no detection of impurities or unwanted structures. On the other hand, Ti^{4+} and Mg^{2+} codoping can reduce the particle size as well as narrow the particle size distribution. Charge-discharge measurements indicate that the cycling stability is significantly improved after doping, especially at relatively high current rates, *e.g.*, retaining 82.4% of initial discharge capacity for the $Li_3V_{1.9}Ti_{0.05}Mg_{0.05}(PO_4)_3$/C cathode at a rate of 0.5 C after 200 cycles between 3.0 and 4.8 V *vs.* Li/Li^+ (**Fig. 11C**).

Recently, doping metal cations (*e.g.*, Na^+ [295], and Ca^{2+} [254]) at the Li sites instead of V sites in the LVP system was also investigated, and some positive impacts on active material utilization and capacity fading were achieved. For example, Chen *et al*. [296] synthesized Na^+-doped $Li_{3-x}Na_xV_2(PO_4)_3$/C (x = 0, 0.03, 0.05 and 0.07) samples by a sol-gel method. Based on the analysis of XRD patterns, the cell volume of Na^+-doped samples is calculated to be somewhat larger than that of pristine one, which is because that the radius of Na^+ (0.97 Å) is larger than that of Li^+ (0.68 Å). Larger cell volume can provide more channel space for Li^+ transportation, leading to higher Li^+ diffusion coefficient,

which is verified by the calculation from GITT method. For example, Li^+ diffusion coefficient of $Li_{2.95}Na_{0.05}V_2(PO_4)_3/C$ is found to be at least three times higher than that of LVP/C. Moreover, the EIS indicates that the charge transfer resistance is largely reduced after Na^+-doping. Therefore, Na^+-doped cathodes display much better electrochemical performance than that of LVP/C, and $Li_{2.95}Na_{0.05}V_2(PO_4)_3/C$ (2.9 wt%) exhibits the highest capacity and the best cycling stability. It can deliver an initial capacity of 173.1 mAh g^{-1} and capacity retention of 91% after 30 cycles at a high rate of 1 C between 3.0 and 4.8 V *vs.* Li/Li^+ (**Fig. 11D**).

In addition to the cation doping, it has been reported that anion doping (*e.g.*, F^- [297], and Cl^- [294]) was also effective in enhancing the electrochemical performance of LVP. For example, the substitution of Cl^- for $(PO4)^{3-}$ in LVP can reduce the charge transfer resistance of electrode and alleviate the polarization under high current densities [294]. Also the strong electronegative of Cl^- might decrease the Li-O bond energy and led to an easily extraction of lithium ions, *e.g.*, showing an increase of two orders of magnitude in lithium ion diffusion coefficient for $Li_3V_2(PO_4)_{2.88}Cl_{0.12}/C$ (6.5 wt%) electrode. As a result, the high-rate capabilities at 5 and 8 C rates are improved significantly by Cl^--doping, *e.g.*, presenting a high discharge capacity of 107 mAh g^{-1} for $Li_3V_2(PO_4)_{2.88}Cl_{0.12}/C$ (6.5 wt%) cathode after 80 cycles at 8 C between 3.0 and 4.3 V *vs.* Li/Li^+ (**Fig. 11E**). Furthermore, cation and anion codoping has been demonstrated recently in LVP. It was reported that Al^{3+} and Cl^--substitution ($Li_3V_{1.98}Al_{0.02}(PO_4)_{2.99}Cl_{0.01}/C$) displays superior rate performance, *e.g.*, delivering a discharge capacity of 103 mAh g^{-1} at 15 C after 100 cycles between 3.0 and 4.8 V *vs.* Li/Li^+ (**Fig. 11F**) [293].

More details about the effect of ion-doping on the electrochemical performance of LVP cathodes are summarized in **Table 2**.

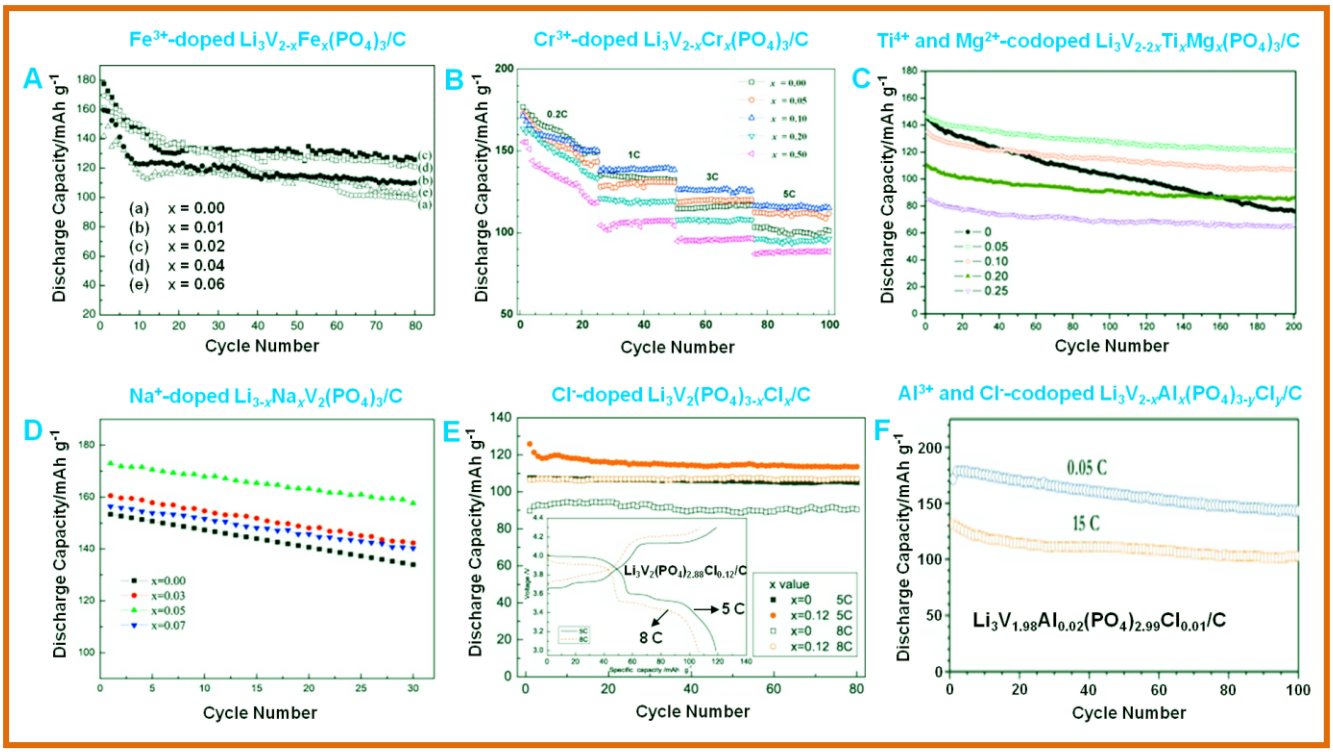

Fig. 11 (A) Cycling performance of $Li_3V_{2-x}Fe_x(PO_4)_3$/C at 0.2 C. Reproduced with permission from [146]. (B) Rate capability of $Li_3V_{2-x}Cr_x(PO_4)_3$/C. Reproduced with permission from [161]. (C) Long-term cycling performance of $Li_3V_{2-2x}Ti_xMg_x(PO_4)_3$/C at 0.5 C. Reproduced with permission from [291]. (D) Cycling performance of $Li_{3-x}Na_xV_2(PO_4)_3$/C at 1 C. Reproduced with permission from [296]. (E) Cycling performance of the pristine LVP/C and $Li_3V_2(PO_4)_{2.88}Cl_{0.12}$/C at 5 and 8 C (inset is the 10^{th} charge-discharge profiles of $Li_3V_2(PO_4)_{2.88}Cl_{0.12}$/C at 5 and 8 C). Reproduced with permission from [294]. (F) Cycling performance of $Li_3V_{1.98}Al_{0.02}(PO_4)_{2.99}Cl_{0.01}$/C at 0.05 and 15 C. Reproduced with permission from [293].

Table 2 The effect of ion-doping on the electrochemical performance of LVP cathodes

Dopants	Optimized composition	Electrochemical Performance	References
Fe^{3+}	$Li_3V_{1.98}Fe_{0.02}(PO_4)_3$/C (1 wt%)	In 3.0-4.9 V, discharge capacities of 177 mAh g^{-1} (1^{st} cycle) and 126 mAh g^{-1} (80^{th} cycle) were obtained at 0.2 C	[146]
Fe^{3+}	$Li_3V_{1.95}Fe_{0.05}(PO_4)_3$/C (11 wt%)	In 3.0-4.8 V, capacities of 174 mAh g^{-1} (1^{st} cycle) and 167 mAh g^{-1} (50^{th} cycle) at 0.1 C as well as 110 mAh g^{-1} at 10 C were achieved	[298]
Cr^{3+}	$Li_3V_{1.9}Cr_{0.1}(PO_4)_3$/C (6.5 wt%)	σ (electronic conductivity) = 2.6×10^{-3} S cm^{-1}. In 3.0-4.8 V, it had capacities of 171 mAh g^{-1} (1^{st} cycle) with 78.6% capacity retention after 100 cycles at 0.2 C and 130 mAh g^{-1} (1^{st} cycle) at 4 C	[161]
Cr^{3+}	$Li_3V_{1.9}Cr_{0.1}(PO_4)_3$/C	In 3.0-4.8 V, initial capacities of 142 mAh g^{-1} at 1 C and 120 mAh g^{-1} at 2 C	[299]
Co^{2+}	$Li_3V_{1.85}Co_{0.15}(PO_4)_3$/C (7.4 wt%)	σ = 2.06×10^{-4} S cm^{-1}. In 3.0-4.8 V, delivering 163.3 mAh g^{-1} (1^{st} cycle) and 73.4% capacity retention after 50 cycles at 0.1 C	[284]
Co^{2+}	$Li_3V_{1.9}Co_{0.1}(PO_4)_3$/C (11 wt%)	In 3.0-4.8 V, showing 178 mAh g^{-1} (1^{st} cycle) with 96% capacity retention after 50 cycles at 0.1 C and 115 mAh g^{-1} at 10 C	[298]
Mg^{2+}	$Li_3V_{1.8}Mg_{0.3}(PO_4)_3$/C (4.4 wt%)	In 3.0-4.3 V, showing 127 mAh g^{-1} (1^{st} cycle) with 91.4% capacity retention after 100 cycles at 1 C	[287]
Mg^{2+}	$Li_3(V_{0.9}Mg_{0.1})_2(PO_4)_3$/C	In 3.0-4.3 V, initial capacity of 107 mAh g^{-1} with 98% capacity retention after 80 cycles at 20 C	[300]
Mn^{2+}	$Li_3V_{1.9}Mn_{0.1}(PO_4)_3$/C	In 3.0-4.8 V, around 90 mAh g^{-1} (4^{th} cycle) at 0.1 C	[285]
Ni^{2+}	$Li_3V_{1.96}Ni_{0.04}(PO_4)_3$/C (4.8 wt%)	In 3.0-4.8 V, initial capacity of 112.1 $mAhg^{-1}$ with capacity retention of 95.2 % after 300 cycles at 10 C	[286]
Al^{3+}	$Li_3V_{1.92}Al_{0.08}(PO_4)_3$/C (4.67 wt%)	In 3.0-4.3 V, 128 mAh g^{-1} (6^{th} cycle) and 93% capacity retention after 200 cycles at 0.5 C In 3.0-4.8 V, 177 mAh g^{-1} (6^{th} cycle) and 82% capacity retention after 200 cycles at 0.5 C	[288]
Al^{3+}	$Li_3V_{1.98}Al_{0.02}(PO_4)_3$/C (0.38 wt%)	In 3.0-4.8 V, showing 187 mAh g^{-1} at 0.1 C and 119 mAh g^{-1} at 20 C	[301]
Al^{3+}	$Li_3V_{1.98}Al_{0.02}(PO_4)_3$/C	In 3.0-4.8 V, ~182 mAh g^{-1} (1^{st} cycle) and 83% capacity retention after 50 cycles were obtained at a current density of 0.1 mA cm^{-2}	[283]
Sc^{3+}	$Li_3V_{1.85}Sc_{0.15}(PO_4)_3$/C	In 3.0-4.3 V, ~75 mAh g^{-1} (1^{st} cycle) at 5 C In 3.0-4.8 V, ~87 mAh g^{-1} (1^{st} cycle) at 5 C	[254]
Ce^{3+}	$Li_3V_{1.95}Ce_{0.05}(PO_4)_3$/C	In 3.0-4.3 V, displaying 88.6 mAh g^{-1} and 94.3% capacity retention after 100 cycles at 10 C	[289]
Sn^{4+}	$Li_3V_{1.95}Sn_{0.05}(PO_4)_3$/C	In 2.5-4.5 V, showing an initial capacity of 136 mAh g^{-1} and 91.2% capacity retention after 80 cycles at 0.5 C	[177]

Mo^{6+}	$Li_3V_{1.97}Mo_{0.03}(PO_4)_3$/C (3.34 wt%)	In 3.0-4.3 V, 122.8 mAh g^{-1} at 10 C and 117.6 mAh g^{-1} at 20 C	[290]
Ti^{4+} and Mg^{2+}	$Li_3V_{1.9}Ti_{0.05}Mg_{0.05}(PO_4)_3$/C	In 3.0-4.8 V, showing 147 mAh g^{-1} (1^{st} cycle) and 82.4% capacity retention after 200 cycles at 0.5 C	[291]
Ti^{4+} and Mn^{2+}	$Li_3V_{1.9}Ti_{0.05}Mn_{0.05}(PO_4)_3$/C (4.19 wt%)	In 3.0-4.8 V, ~110 mAh g^{-1} (1^{st} cycle) and ~66% capacity retention after 160 cycles at 5 C	[292]
Ti^{4+} and Fe^{2+}	$Li_3V_{1.9}Ti_{0.05}Fe_{0.05}(PO_4)_3$/C (4.16 wt%)	In 3.0-4.8 V, ~127 mAh g^{-1} (1^{st} cycle) and ~82% capacity retention after 160 cycles at 5 C	[292]
Ca^{2+}	$Li_{2.96}Ca_{0.02}V_2(PO_4)_3$/C	In 3.0-4.3 V, ~76 mAh g^{-1} (1^{st} cycle) at 5 C In 3.0-4.8 V, ~80 mAh g^{-1} (1^{st} cycle) at 5 C	[254]
Na^{+}	$Li_{2.97}Na_{0.03}V_2(PO_4)_3$/C (6.5 wt%)	$\sigma = 6.74 \times 10^{-3}$ S cm^{-1}. In 3.0-4.8 V, exhibiting 119 mAh g^{-1} (1^{st} cycle) and 88% capacity retention after 80 cycles at 2 C	[295]
Na^{+}	$Li_{2.95}Na_{0.05}V_2(PO_4)_3$/C (2.9 wt%)	In 3.0-4.8 V, 187 and 173.1 mAh g^{-1} (1^{st} cycle) and 95.3% and 91% capacity retention after 30 cycles at 0.2 and 1 C, respectively	[296]
F^{-}	$Li_3V_2(PO_4)_{2.9}F_{0.1}$/C	$\sigma = 7.2 \times 10^{-6}$ S cm^{-1}. In 3.0-4.2 V, showing initial capacity of 117 mAh g^{-1} at 10 C and ~ 90.6% capacity retention after 30 cycles	[297]
Cl^{-}	$Li_3V_2(PO_4)_{2.88}Cl_{0.12}$/C (6.5 wt%)	In 3.0-4.3 V, showing 107 mAh g^{-1} at 8 C	[294]
Al^{3+} and Cl^{-}	$Li_3V_{1.98}Al_{0.02}(PO_4)_{2.99}Cl_{0.01}$/C	In 3.0-4.8 V, 130 mAh g^{-1} (1^{st} cycle) with a capacity retention of 79% after 100 cycles at 15 C	[293]

6.5. Designing nanostructures

Recently, nanostructured materials are highly attractive for LIBs as they can offer a range of unique advantages over their traditional counterparts including: (1) a large electrode/electrolyte contact area and short path lengths for Li^{+} and electronic transport, leading to high charge-discharge rates; (2) easy accommodation of the strain of lithium insertion/extraction, improving the rechargeability of the batteries [302-306]. Over the recent years, much effort has been made to improve the power performance of LVP by constructing nanostructured electrodes.

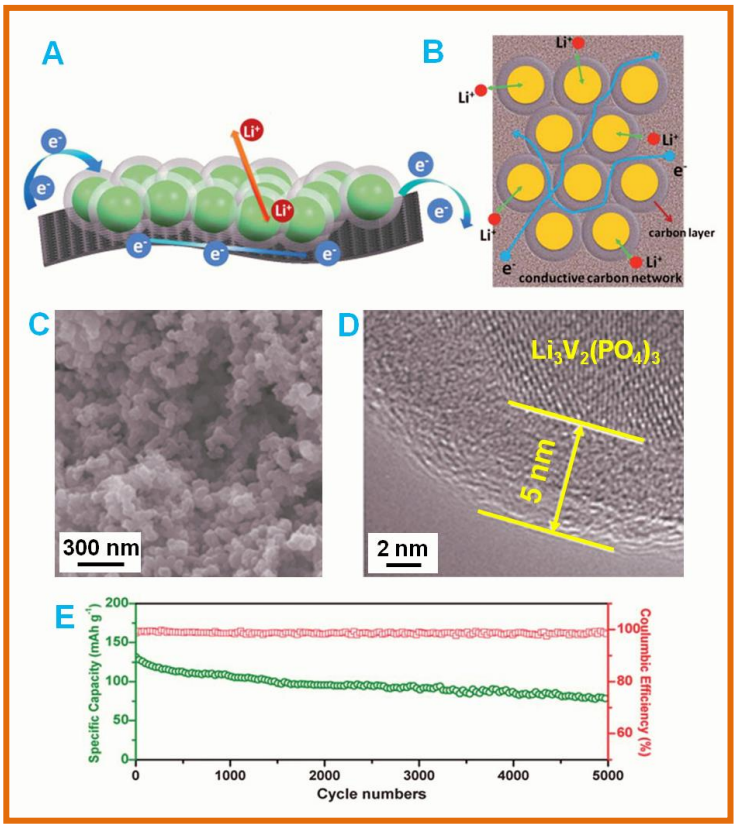

Fig. 12 Schematic illustration of facile electron and lithium transport in LVP nanospheres with continuous carbon network and carbon coating layer (A) and top cross-section view (B). SEM image (C) and corresponding HRTEM image (D) of the sample prepared with 20 wt% PEG-4000. (E) Its cycling performance at 5 C rate for 5000 cycles. Reproduced with permission from [307].

Mai *et al*. [307] reported a rationally controllable way to synthesize LVP/C nanospheres using acetylene black as the template and PEG-4000 as the surface modification reactant. During the synthesis process, acetylene black can form a carbon network to provide a facile and continuous pathway for electron transport, leading to enhanced conductivity of the electrode, and PEG-4000 is pyrolyzed to form a homogeneous carbon layer (the thickness is tuned by adjusting the PEG amount), which not only can further improve the conductivity but also restrains the particle growth to maintain the LVP particles at the nanoscale (**Fig. 12A and B**). The SEM image (**Fig. 12C**) shows that the diameters of nanospheres

prepared with 20 wt% PEG-4000 are 40-60 nm with good uniformity, and corresponding HRTEM image (**Fig. 12D**) reveals that the thickness of carbon coating layer is around 5 nm. This nanosized material with continuous carbon network and carbon coating layer demonstrates promising high-rate and long-life energy storage performance, *e.g.*, showing a capacity retention of up to 83% of initial capacity (132 mAh g^{-1}) after 1000 cycles at a rate of 5 C between 3.0 and 4.5 V *vs.* Li/Li^+, and retaining a capacity of 79 mAh g^{-1} even after 5000 cycles (**Fig. 12E**).

Pan *et al*. [253] described a one-step preparation procedure for fabricating LVP/C nanobelts. The procedure was based on a solid-state reaction in a molten surfactant-paraffin media. As seen from **Fig. 13A**, the as-prepared LVP/C nanobelts have the thickness of around 50 nm, width of ~200 nm, and length of ~500 nm. Oleic acid [$(CH_3(CH_2)_7CH=CH(CH_2)_7COOH)$], a mono-unsaturated omega-9 fatty acid, plays an important role to form the nanobelt. It can act as the surface-capping ligand of precursors with its carboxylic group to direct the 1D growth orientation of LVP in the molten paraffin media. When charged/discharged in a voltage range between 3.0 and 4.3V *vs.* Li/Li^+, the LVP/C nanobelts deliver capacities of 131, 128, 122, and 110 mAh g^{-1} at rates of 1, 2, 4, and 8 C, respectively (**Fig. 13B**).

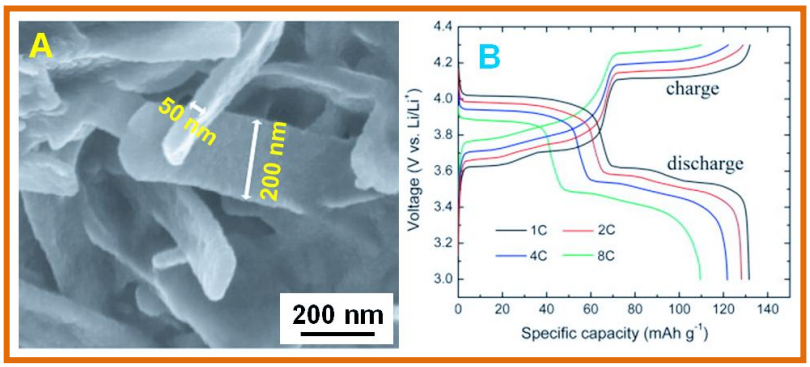

Fig. 13 (A) High magnification SEM image of LVP/C nanobelts. (B) Discharge/charge curves of LVP/C nanobelts at various C-rates. Reproduced with permission from [253].

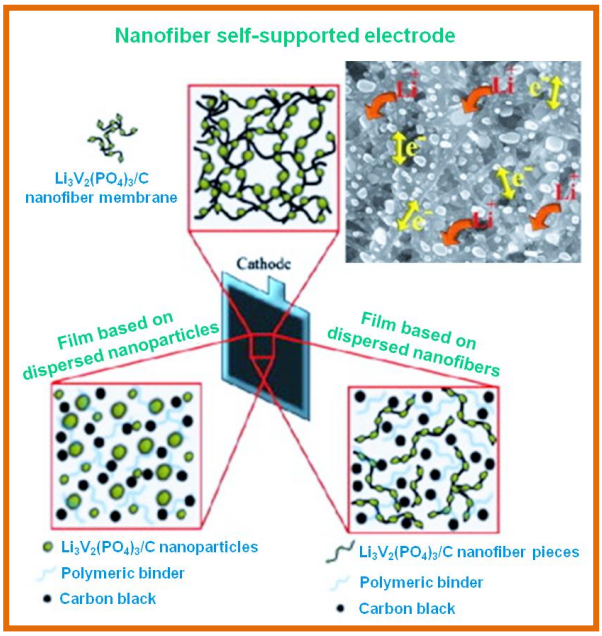

Fig. 14 Schematic illustration of three different electrodes (nanofiber self-supported electrode, film electrodes based on dispersed nanofibers and nanoparticles). Reproduced with permission from [308].

Hagen *et al.* [308] designed a novel alkoxide-based precursor sol containing lithium isopropoxide, vanadylisopropoxide, dibutyl phosphate, acetic acid and PVP to produce LVP/C nanofibers by sol-gel electrospinning technique. Besides, the precursor mixture was also suitable for fabricating isotropic shaped LVP/C nanoparticles by conventional sol-gel processing. The as-obtained porous and interconnected nanofibrous networks and nanoparticles can be used for preparation of differently textured electrodes (**Fig. 14**) to analyze the influence of electrode texture and morphology on the electrochemical performances. The self-supporting electrodes were prepared by casting LVP/C nanofiber networks onto aluminum foil without addition of binder or carbon black. The conventional film electrodes were prepared by milling of LVP/C composites (electrospun nanofibers or sol-gel nanoparticles) with carbon black and PVDF binder. The electrochemical evaluation reveals that the self-supporting nanofiber cathode has the best rate

capability, *e.g.*, 99 mAh g^{-1} at 2 C between 3.0 and 4.3V *vs.* Li/Li^+, whereas the film electrode based on nanoparticles shows the largest polarization. The self-supported electrospun nanofiber electrode takes benefits of the porous and highly accessible structure, where the electrolyte wetting and thereby the electrode kinetics can be accelerated and furthermore a homogenous incorporation of the conductive carbon backbone offers 3D percolation pathways.

Qiao *et al*. [158] reported the synthesis of LVP/C nanoplates *via* a solution route followed by solid-state reaction. It is observed from **Fig. 15** that the as-obtained LVP/C nanoplates have lateral dimensions of 2-10 μm, and thicknesses of 40-100 nm. As seen from HRTEM image (**Fig. 15D**), a uniform carbon layer with the thickness of around 5.3 nm is presented on the surfaces of LVP plate. The carbon content is determined to be 3.22 wt% by the elemental analysis. At a charge-discharge rate of 3 C, the LVP/C nanoplates exhibit an initial discharge capacity of 125.2 and 133.1 mAh g^{-1} in the voltage ranges of 3.0-4.3 and 3.0-4.8 V *vs.* Li/Li^+, respectively. After 500 cycles, the electrodes still can deliver discharge capacities of 111.8 and 97.8 mAh g^{-1} correspondingly, showing excellent cycling stability.

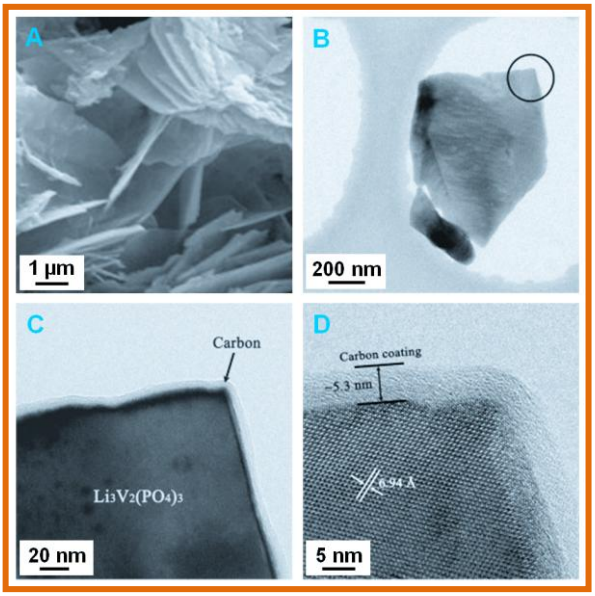

Fig. 15 SEM (A), TEM (B, C), and HRTEM (D) images of LVP/C nanoplates. Reproduced with permission from [158].

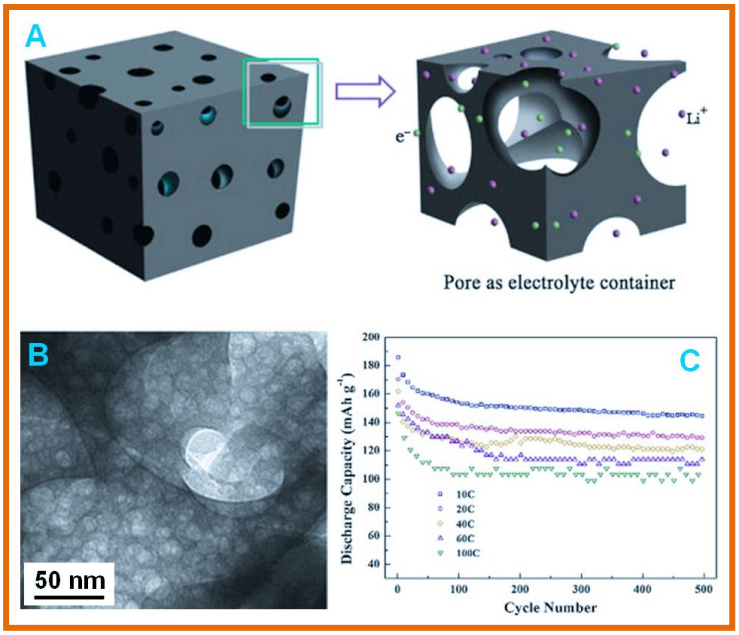

Fig. 16 (A) Schematic illustration of the porous LVP/C composite for facile electrolyte penetration. (B) TEM image of porous precursor. (C) Cycling performance of porous LVP/C from 10 to 100 C between 3.0 and 4.8 V *vs.* Li/Li^+. Reproduced with permission from [309].

Zhang *et al*. [309] designed a structure of pore-containing nano-sized LVP particles with a thin carbon layer covering all the surfaces to improve the electrochemical performance. It combines the advantages of porous structure and carbon-coating. As illustrated in **Fig. 16A**, the pores serve as fast channels for lithium ion transport and reduce the distance of lithium ion diffusion, resulting in improved ionic conductivity for LVP. Additionally, the carbon-coating can improve the electron conductivity and prevent the aggregation of nanoparticles. A sol-gel-combustion method was employed to synthesize such porous LVP/C composite. Firstly, a porous precursor was obtained during the combustion process due to the degradation of chelates or citrate anion. Then the porous precursor was mixed with the sucrose and calcined at 800 ^{o}C. The carbon pyrolyzed from sucrose could deposit on the wall of pores and surface of particle to form

carbon coating. TEM image (**Fig. 16B**) reveals that the as-obtained precursor exhibits a spongy-shaped porous network structure, and the diameter of the pores is about 20-30 nm. After the calcination with sucrose, the porous structure is kept, and the LVP nanocrystals embed in the carbon matrix. The carbon content is estimated to be 5.4 wt% by the element analysis. In the potential range of 3.0-4.3 V *vs.* Li/Li^+, discharge capacities of 122, 114, 108 and 88 mAh g^{-1} can be delivered at rates of 10, 20, 40 and 60 C after 100 cycles, respectively. In the potential range of 3.0-4.8 V *vs.* Li/Li^+ (**Fig. 16C**), discharge capacities of 145, 129, 122, 114 and 103 mAh g^{-1} are obtained after 500 cycles at high rates of 10, 20, 40, 60 and 100 C, respectively.

7. Conclusions and prospects

Since the advent of LIBs in 1991, positive electrode (cathode) materials has received tremendous attention and research interest. To fulfill the newly emerging applications, such as powering EVs/HEVs and portable electronics, advanced cathode materials with superior integrated performance that enables high energy and power density and environmentally benign are highly demanded. Monoclinic LVP with promising electrochemical properties including excellent cycling stability, high theoretical capacity (197 mAh g^{-1}), low synthetic cost, improved safety characteristic, and low environmental impact has emerged as a highly suitable candidate for the cathodes of the next-generation LIBs.

In this review article, we discuss the development and challenges for the LVP cathode material, including the host structure, mechanism of lithium insertion/extraction, transport properties (*i.e.*, electronic conductivity, and lithium diffusion), synthesis and electrochemical properties. Synthesis procedures are mainly focused on controlling the morphology, and optimizing particle size through technologies of solid state reaction, sol-gel chemistry, hydrothermal, and spray pyrolysis, *etc*. The relatively low ionic and electronic conductivity of LVP compound bring to the forefront

the importance of conductive coatings and additives including carbon coating, graphene modification, *etc*., ion-doping, and nanoscale engineering to mitigate the shortcomings.

Although the performance of LVP is improved and understood step by step, some fundamental questions still remain and need to be investigated in detail. Regarding to the large-scale battery applications, a simple, reliable, cheap, less wasteful synthetic method for LVP is highly desirable. The wet chemical preparation route, such as sol-gel and hydrothermal, has great potential for manufacturing nano-sized LVP. This method, however, has some drawbacks such as strict reaction conditions to restrict its industrially mass production. It is thus necessary to further optimize and modify the current wet process. In the future, it is also anticipated that LVP continues its improvement of electrochemical properties with carbon coating, ion-doping, nanocrystallization, or material processing. The introduction of too much carbon leads to a significant decrease of the energy density, especially for the volumetric energy density. A uniform and complete carbon coating throughout the LVP powder is highly attractive, which ensures LVP particles transfer electrons through all directions and alleviate the polarization phenomenon, and finally reduce the usage of carbon. Additionally, carbon coating is better to be porous to allow easy penetration of lithium ions. Low-level doping of LVP by a range of cations and anions is proven to be an effective route to improve the rate capability and cycle stability. An in-depth understanding on the principles of ion-doping, *e.g.*, the precise site occupancy of specific dopants, is necessary. Furthermore, the nanostructured LVP materials has drawn more attention recently due to its remarkable rate capability. There, however, still remain plenty of opportunities for designing novel nanoarchitectures and morphology to further increase battery energy/power densities, enhance charge/discharge rate capability, improve service life and safety, and reduce the cost at the same time. Further work is also required to understand the mechanisms of lithium storage in nanomaterials and kinetic transport on the interface between electrode and electrolyte. The development of matched electrolyte systems is equally essential, especially for high-voltage (> 4.5 V *vs.* Li/Li^+)

operation. As required by EVs/HEVs, it is better for LVP batteries to be able to operate well at the high and low temperatures. With worldwide efforts, the material chemistry and electrochemistry of this attractive cathode material are believed to be further enhanced and enriched.

Acknowledgements

The authors gratefully acknowledge, NRF2009EWT-CERP001-026 (Singapore), A*STAR SERC grant 1021700144 and Singapore MPA 23/04.15.03 grant, and Singapore National Research Foundation under CREATE program: EMobility in Megacities.

References

[1] E. Karden, S. Ploumen, B. Fricke, T. Miller, K. Snyder, J. Power Sources 168 (2007) 2.

[2] S. Linic, P. Christopher, D.B. Ingram, Nat. Mater. 10 (2011) 911.

[3] C. Liu, F. Li, L.P. Ma, H.M. Cheng, Adv. Mater. 22 (2010) E28.

[4] X.H. Rui, Z.Y. Lu, Z.Y. Yin, D.H. Sim, N. Xiao, T.M. Lim, H.H. Hng, H. Zhang, Q.Y. Yan, Small 9 (2013) 716.

[5] X.H. Rui, M.O. Oo, D.H. Sim, S.C. Raghu, Q.Y. Yan, T.M. Lim, M. Skyllas-Kazacos, Electrochim. Acta 85 (2012) 175.

[6] X.H. Rui, A. Parasuraman, W.L. Liu, D.H. Sim, H.H. Hng, Q.Y. Yan, T.M. Lim, M. Skyllas-Kazacos, Carbon 64 (2013) 464.

[7] J.X. Zhu, Z.Y. Yin, H. Li, H.T. Tan, C.L. Chow, H. Zhang, H.H. Hng, J. Ma, Q.Y. Yan, Small 7 (2011) 3458.

[8] J.M. Tarascon, M. Armand, Nature 414 (2001) 359.

[9] A.S. Arico, P. Bruce, B. Scrosati, J.M. Tarascon, W. Van Schalkwijk, Nat. Mater. 4 (2005) 366.

[10] M.S. Whittingham, Chem. Rev. 104 (2004) 4271.

[11] P.G. Bruce, B. Scrosati, J.M. Tarascon, Angew. Chem. Int. Ed. 47 (2008) 2930.

[12] J.B. Goodenough, Y. Kim, Chem. Mater. 22 (2010) 587.

[13] X.H. Rui, Y. Jin, X.Y. Feng, L.C. Zhang, C.H. Chen, J. Power Sources 196 (2011) 2109.

[14] R. Cai, H. Liu, W.Y. Zhang, H.T. Tan, D. Yang, Y.Z. Huang, H.H. Hng, T.M. Lim, Q.Y. Yan, Small 9 (2013) 1036.

[15] S. Megahed, B. Scrosati, J. Power Sources 51 (1994) 79.

[16] D. Guyomard, J.M. Tarascon, Adv. Mater. 6 (1994) 408.

[17] K. Xu, Chem. Rev. 104 (2004) 4303.

[18] Y. Wang, G.Z. Cao, Adv. Mater. 20 (2008) 2251.

[19] L.W. Ji, Z. Lin, M. Alcoutlabi, X.W. Zhang, Energy Environ. Sci. 4 (2011) 2682.

[20] Y.G. Guo, J.S. Hu, L.J. Wan, Adv. Mater. 20 (2008) 2878.

[21] S. Megahed, W. Ebner, J. Power Sources 54 (1995) 155.

[22] F.Y. Cheng, J. Liang, Z.L. Tao, J. Chen, Adv. Mater. 23 (2011) 1695.

[23] Z.Y. Lu, J.X. Zhu, D.H. Sim, W.W. Zhou, W.H. Ship, H.H. Hng, Q.Y. Yan, Chem. Mater. 23 (2011) 5293.

[24] C.K. Chan, H.L. Peng, G. Liu, K. McIlwrath, X.F. Zhang, R.A. Huggins, Y. Cui, Nat. Nanotechnol. 3 (2008) 31.

[25] A. Magasinski, P. Dixon, B. Hertzberg, A. Kvit, J. Ayala, G. Yushin, Nat. Mater. 9 (2010) 353.

[26] M.H. Park, M.G. Kim, J. Joo, K. Kim, J. Kim, S. Ahn, Y. Cui, J. Cho, Nano Lett. 9 (2009) 3844.

[27] Y. Idota, T. Kubota, A. Matsufuji, Y. Maekawa, T. Miyasaka, Science, 276 (1997) 1395.

[28] K.T. Lee, Y.S. Jung, S.M. Oh, J. Am. Chem. Soc. 125 (2003) 5652.

[29] C.M. Park, J.H. Kim, H. Kim, H.J. Sohn, Chem. Soc. Rev. 39 (2010) 3115.

[30] X. Huang, J. Chen, H. Yu, S.J. Peng, R. Cai, Q.Y. Yan, H.H. Hng, RSC Adv. 3 (2013) 5310.

[31] S. Saadat, Y.Y. Tay, J.X. Zhu, P.F. Teh, S. Maleksaeedi, M.M. Shahjamali, M. Shakerzadeh, M. Srinivasan, B.Y. Tay, H.H. Hng, J. Ma, Q.Y. Yan, Chem. Mater. 23 (2011) 1032.

[32] S. Saadat, J.X. Zhu, M.M. Shahjamali, S. Maleksaeedi, Y.Y. Tay, B.Y. Tay, H.H. Hng, J. Ma, Q.Y. Yan, Chem. Commun. 47 (2011) 9849.

[33] H. Kim, J. Cho, Chem. Mater. 20 (2008) 1679.

[34] S.F. Fan, T. Sun, X.H. Rui, Q.Y. Yan, H.H. Hng, J. Power Sources 201 (2012) 288.

[35] P.R. Abel, A.M. Chockla, Y.M. Lin, V.C. Holmberg, J.T. Harris, B.A. Korgel, A. Heller, C.B. Mullins, ACS Nano, 7 (2013) 2249.

[36] C.K. Chan, X.F. Zhang, Y. Cui, Nano Lett. 8 (2008) 307.

[37] Y. Yu, C.L. Yan, L. Gu, X.Y. Lang, K. Tang, L. Zhang, Y. Hou, Z.F. Wang, M.W. Chen, O.G. Schmidt, J. Maier, Adv. Energy Mater. 3 (2013) 281.

[38] L.P. Tan, Z.Y. Lu, H.T. Tan, J.X. Zhu, X.H. Rui, Q.Y. Yan, H.H. Hng, J. Power Sources 206 (2012) 253.

[39] W.H. Shi, X.H. Rui, J.X. Zhu, Q.Y. Yan, J. Phys. Chem. C, 116 (2012) 26685.

[40] X.W. Lou, Y. Wang, C.L. Yuan, J.Y. Lee, L.A. Archer, Adv. Mater. 18 (2006) 2325.

[41] M.S. Park, G.X. Wang, Y.M. Kang, D. Wexler, S.X. Dou, H.K. Liu, Angew. Chem. Int. Ed. 46 (2007) 750.

[42] X. Huang, J. Chen, H. Yu, R. Cai, S.J. Peng, Q.Y. Yan, H.H. Hng, J. Mater. Chem. A 1 (2013) 6901.

[43] J.X. Zhu, Z.Y. Yin, D. Yang, T. Sun, H. Yu, H.E. Hoster, H.H. Hng, H. Zhang, Q.Y. Yan, Energy Environ. Sci. 6 (2013) 987.

[44] J.X. Zhu, T. Zhu, X.Z. Zhou, Y.Y. Zhang, X.W. Lou, X.D. Chen, H. Zhang, H.H. Hng, Q.Y. Yan, Nanoscale 3 (2011) 1084.

[45] C. Xu, Y. Zeng, X.H. Rui, N. Xiao, J.X. Zhu, W.Y. Zhang, J. Chen, W.L. Liu, H.T. Tan, H.H. Hng, Q.Y. Yan, ACS

Nano 6 (2012) 4713.

[46] S. Saadat, J.X. Zhu, D.H. Sim, H.H. Hng, R. Yazami, Q.Y. Yan, J. Mater. Chem. A 1 (2013) 8672.

[47] X.H. Rui, H.T. Tan, D.H. Sim, W.L. Liu, C. Xu, H.H. Hng, R. Yazami, T.M. Lim, Q.Y. Yan, J. Power Sources 222 (2013) 97.

[48] J.X. Zhu, Y.K. Sharma, Z.Y. Zeng, X.J. Zhang, M. Srinivasan, S. Mhaisalkar, H. Zhang, H.H. Hng, Q.Y. Yan, J. Phys. Chem. C 115 (2011) 8400.

[49] H.W. Shim, Y.H. Jin, S.D. Seo, S.H. Lee, D.W. Kim, ACS Nano 5 (2011) 443.

[50] P. Poizot, S. Laruelle, S. Grugeon, L. Dupont, J.M. Tarascon, Nature 407 (2000) 496.

[51] W.Y. Zhang, Y. Zeng, N. Xiao, H.H. Hng, Q.Y. Yan, J. Mater. Chem. 22 (2012) 8455.

[52] C.M. Zhang, J. Chen, Y. Zeng, X.H. Rui, J.X. Zhu, W.Y. Zhang, C. Xu, T.M. Lim, H.H. Hng, Q.Y. Yan, Nanoscale 4 (2012) 3718.

[53] Y.G. Li, B. Tan, Y.Y. Wu, Nano Lett. 8 (2008) 265.

[54] H.W. Huang, Y. Liu, J.H. Wang, M.X. Gao, X.S. Peng, Z.Z. Ye, Nanoscale 5 (2013) 1785.

[55] B.L. Ellis, K.T. Lee, L.F. Nazar, Chem. Mater. 22 (2010) 691.

[56] J.W. Fergus, J. Power Sources 195 (2010) 939.

[57] K. Mizushima, P.C. Jones, P.J. Wiseman, J.B. Goodenough, Mater. Res. Bull. 15 (1980) 783.

[58] J.N. Reimers, J.R. Dahn, J. Electrochem. Soc. 139 (1992) 2091.

[59] O.C. Compton, A. Abouimrane, Z. An, M.J. Palmeri, L.C. Brinson, K. Amine, S.T. Nguyen, Small 8 (2012) 1110.

[60] X. Pa, C.H. Yu, Nanoscale 4 (2012) 6743.

[61] E. Antolini, Solid State Ionics 170 (2004) 159.

[62] T. Ohzuku, Y. Makimura, Chem. Lett. (2001) 642.

[63] C.F. Yang, J.J. Huang, L.G. Huang, G.J. Wang, J. Power Sources 226 (2013) 219.

[64] T. Mei, Y.C. Zhu, K.B. Tang, Y.T. Qian, RSC Adv. 2 (2012) 12886.

[65] J. Choi, A. Manthiram, Electrochem. Solid State Lett. 8 (2005) C102.

[66] J.M. Tarascon, E. Wang, F.K. Shokoohi, W.R. McKinnon, S. Colson, J. Electrochem. Soc. 138 (1991) 2859.

[67] Y.M. Wu, Z.H. Wen, H.B. Feng, J.H. Li, Small 8 (2012) 858.

[68] Y.L. Ding, J.A. Xie, G.S. Cao, T.J. Zhu, H.M. Yu, X.B. Zhao, Adv. Funct. Mater. 21 (2011) 348.

[69] W. Tang, Y.Y. Hou, F.X. Wang, L.L. Liu, Y.P. Wu, K. Zhu, Nano Lett. 13 (2013) 2036.

[70] R.J. Gummow, A. Dekock, M.M. Thackeray, Solid State Ionics 69 (1994) 59.

[71] B.H. Deng, H. Nakamura, M. Yoshio, J. Power Sources 180 (2008) 864.

[72] K.Y. Chung, K.B. Kim, Electrochim. Acta 49 (2004) 3327.

[73] R. Santhanam, B. Rambabu, J. Power Sources, 195 (2010) 5442.

[74] Q.M. Zhong, A. Bonakdarpour, M.J. Zhang, Y. Gao, J.R. Dahn, J. Electrochem. Soc. 144 (1997) 205.

[75] J.C. Arrebola, A. Caballero, M. Cruz, L. Hernan, J. Morales, E.R. Castellon, Adv. Funct. Mater. 16 (2006) 1904.

[76] X.L. Zhang, F.Y. Cheng, K. Zhang, Y.L. Liang, S.Q. Yang, J. Liang, J. Chen, RSC Adv. 2 (2012) 5669.

[77] Y.C. Dong, Z.B. Wang, H. Qin, X.L. Sui, RSC Adv. 2 (2012) 11988.

[78] Z.Y. Lu, X.H. Rui, H.T. Tan, W.Y. Zhang, H.H. Hng, Q.Y. Yan, ChemPlusChem 78 (2013) 218.

[79] R. Alcantara, M. Jaraba, P. Lavela, J.L. Tirado, Electrochim. Acta 47 (2002) 1829.

[80] B. Xu, D.N. Qian, Z.Y. Wang, Y.S.L. Meng, Mater. Sci. Eng. R. 73 (2012) 51.

[81] A.M. Cao, J.S. Hu, H.P. Liang, L.J. Wan, Angew. Chem. Int. Ed. 44 (2005) 4391.

[82] X.H. Rui, Z.Y. Lu, H. Yu, D. Yang, H.H. Hng, T.M. Lim, Q.Y. Yan, Nanoscale 5 (2013) 556.

[83] Y. Wang, G.Z. Cao, Chem. Mater. 18 (2006) 2787.

[84] S. Zhou, X.G. Yang, Y.J. Lin, J. Xie, D.W. Wang, ACS Nano 6 (2012) 919.

[85] X.H. Rui, J.X. Zhu, W.L. Liu, H.T. Tan, D.H. Sim, C. Xu, H. Zhang, J. Ma, H.H. Hng, T.M. Lim, Q.Y. Yan, RSC Adv. 1 (2011) 117.

[86] X.H. Rui, J.X. Zhu, D. Sim, C. Xu, Y. Zeng, H.H. Hng, T.M. Lim, Q.Y. Yan, Nanoscale 3 (2011) 4752.

[87] A.K. Padhi, K.S. Nanjundaswamy, J.B. Goodenough, J. Electrochem. Soc. 144 (1997) 1188.

[88] A. Yamada, N. Iwane, Y. Harada, S. Nishimura, Y. Koyama, I. Tanaka, Adv. Mater. 22 (2010) 3583.

[89] N. Recham, J.N. Chotard, L. Dupont, C. Delacourt, W. Walker, M. Armand, J.M. Tarascon, Nat. Mater. 9 (2010) 68.

[90] M. Ati, M.T. Sougrati, G. Rousse, N. Recham, M.L. Doublet, J.C. Jumas, J.M. Tarascon, Chem. Mater. 24 (2012) 1472.

[91] P. Barpanda, M. Ati, B.C. Melot, G. Rousse, J.N. Chotard, M.L. Doublet, M.T. Sougrati, S.A. Corr, J.C. Jumas, J.M. Tarascon, Nat. Mater. 10 (2011) 772.

[92] A. Nyten, A. Abouimrane, M. Armand, T. Gustafsson, J.O. Thomas, Electrochem. Commun. 7 (2005) 156.

[93] M.S. Islam, R. Dominko, C. Masquelier, C. Sirisopanaporn, A.R. Armstrong, P.G. Bruce, J. Mater. Chem. 21 (2011) 9811.

[94] D. Rangappa, K.D. Murukanahally, T. Tomai, A. Unemoto, I. Honma, Nano Lett. 12 (2012) 1146.

[95] D.P. Lv, J.Y. Bai, P. Zhang, S.Q. Wu, Y.X. Li, W. Wen, Z. Jiang, J.X. Mi, Z.Z. Zhu, Y. Yang, Chem. Mater. 25 (2013) 2014.

[96] D.A. Cogswell, M.Z. Bazant, ACS Nano 6 (2012) 2215.

[97] S.Y. Chung, J.T. Bloking, Y.M. Chiang, Nat. Mater. 1 (2002) 123.

[98] B. Kang, G. Ceder, Nature 458 (2009) 190.

[99] J.J. Wang, X.L. Sun, Energy Environ. Sci. 5 (2012) 5163.

[100] W.J. Zhang, J. Power Sources 196 (2011) 2962.

[101] K. Zaghib, A. Guerfi, P. Hovington, A. Vijh, M. Trudeau, A. Mauger, J.B. Goodenough, C.M. Julien, J. Power Sources 232 (2013) 357.

[102] D. Carriazo, M.D. Rossell, G.B. Zeng, I. Bilecka, R. Erni, M. Niederberger, Small 8 (2012) 2231.

[103] Y.G. Wang, Y.R. Wang, E.J. Hosono, K.X. Wang, H.S. Zhou, Angew. Chem. Int. Ed. 47 (2008) 7461.

[104] X.H. Rui, X.X. Zhao, Z.Y. Lu, H.T. Tan, D.H. Sim, H.H. Hng, R. Yazami, T.M. Lim, Q.Y. Yan, ACS Nano 7 (2013) 5637.

[105] M. Pivko, M. Bele, E. Tchernychova, N.Z. Logar, R. Dominko, M. Gaberscek, Chem. Mater. 24 (2012) 1041.

[106] N.N. Bramnik, K. Nikolowski, C. Baehtz, K.G. Bramnik, H. Ehrenberg, Chem. Mater. 19 (2007) 908.

[107] J. Wolfenstine, J. Allen, J. Power Sources 142 (2005) 389.

[108] M.Y. Saidi, J. Barker, H. Huang, J.L. Swoyer, G. Adamson, Electrochem. Solid State Lett. 5 (2002) A149.

[109] M. Hu, X.L. Pang, Z. Zhou, J. Power Sources 237 (2013) 229.

[110] J. Gopalakrishnan, K.K. Rangan, Chem. Mater. 4 (1992) 745.

[111] D. Morgan, G. Ceder, M.Y. Saidi, J. Barker, J. Swoyer, H. Huang, G. Adamson, Chem. Mater. 14 (2002) 4684.

[112] A.K. Padhi, K.S. Nanjundaswamy, C. Masquelier, J.B. Goodenough, J. Electrochem. Soc. 144 (1997) 2581.

[113] S.C. Yin, H. Grondey, P. Strobel, M. Anne, L.F. Nazar, J. Am. Chem. Soc. 125 (2003) 10402.

[114] J. Gaubicher, C. Wurm, G. Goward, C. Masquelier, L. Nazar, Chem. Mater. 12 (2000) 3240.

[115] A.S. Andersson, B. Kalska, P. Eyob, D. Aernout, L. Haggstrom, J.O. Thomas, Solid State Ionics 140 (2001) 63.

[116] C. Masquelier, C. Wurm, J. Rodriguez-Carvajal, J. Gaubicher, L. Nazar, Chem. Mater. 12 (2000) 525.

[117] K.S. Nanjundaswamy, A.K. Padhi, J.B. Goodenough, S. Okada, H. Ohtsuka, H. Arai, J. Yamaki, Solid State Ionics 92 (1996) 1.

[118] F. Dyvoire, M. Pintardscrepel, E. Bretey, M. Delarochere, Solid State Ionics 9-10 (1983) 851.

[119] E.A. Genkina, L.A. Muradyan, B.A. Maximov, B.V. Merinov, S.E. Sigarev, Kristallografiya 32 (1987) 74.

[120] S. Patoux, C. Wurm, M. Morcrette, G. Rousse, C. Masquelier, J. Power Sources 119 (2003) 278.

[121] H. Huang, S.C. Yin, T. Kerr, N. Taylor, L.F. Nazar, Adv. Mater. 14 (2002) 1525.

[122] M.Y. Saidi, J. Barker, H. Huang, J.L. Swoyer, G. Adamson, J. Power Sources 119 (2003) 266.

[123] P. Fu, Y.M. Zhao, Y.Z. Dong, X.N. An, G.P. Shen, J. Power Sources 162 (2006) 651.

[124] L.S. Cahill, R.P. Chapman, J.F. Britten, G.R. Goward, J. Phys. Chem. B 110 (2006) 7171.

[125] V.W.J. Verhoeven, I.M. de Schepper, G. Nachtegaal, A.P.M. Kentgens, E.M. Kelder, J. Schoonman, F.M. Mulder, Phys. Rev. Lett. 86 (2001) 4314.

[126] A.B. Bykov, A.P. Chirkin, L.N. Demyanets, S.N. Doronin, E.A. Genkina, A.K. Ivanovshits, I.P. Kondratyuk, B.A. Maksimov, O.K. Melnikov, L.N. Muradyan, V.I. Simonov, V.A. Timofeeva, Solid State Ionics 38 (1990) 31.

[127] H. Ohkawa, K. Yoshida, M. Saito, K. Uematsu, K. Toda, M. Sato, Chem. Lett. (1999) 1017.

[128] M. Sato, H. Ohkawa, K. Yoshida, M. Saito, K. Uematsu, K. Toda, Solid State Ionics 135 (2000) 137.

[129] N. Membreno, P.H. Xiao, K.S. Park, J.B. Goodenough, G. Henkelman, K.J. Stevenson, J. Phys. Chem. C 117 (2013) 11994.

[130] M. Morcrette, J.B. Leriche, S. Patoux, C. Wurm, C. Masquelier, Electrochem. Solid State Lett. 6 (2003) A80.

[131] C.M. Burba, R. Frech, Solid State Ionics 177 (2007) 3445.

[132] Y.H. Lu, L. Wang, J. Song, D.W. Zhang, M.W. Xu, J.B. Goodenough, J. Mater. Chem. A 1 (2013) 68.

[133] S.C. Yin, H. Grondey, P. Strobel, H. Huang, L.F. Nazar, J. Am. Chem. Soc. 125 (2003) 326.

[134] J. Yoon, S. Muhammad, D. Jang, N. Sivakumar, J. Kim, W.H. Jang, Y.S. Lee, Y.U. Park, K. Kang, W.S. Yoon, J. Alloys Compd. 569 (2013) 76.

[135] S.C. Yin, P.S. Strobel, H. Grondey, L.F. Nazar, Chem. Mater. 16 (2004) 1456.

[136] A.S. Andersson, B. Kalska, L. Haggstrom, J.O. Thomas, Solid State Ionics 130 (2000) 41.

[137] X.H. Rui, C. Li, C.H. Chen, Electrochim. Acta 54 (2009) 3374.

[138] G. Yang, H.D. Liu, H.M. Ji, Z.Z. Chen, X.F. Jiang, Electrochim. Acta 55 (2010) 2951.

[139] Q.Q. Chen, J.M. Wang, Z. Tang, W.C. He, H.B. Shao, J.Q. Zhang, Electrochim. Acta 52 (2007) 5251.

[140] M.S. Whittingham, Y.N. Song, S. Lutta, P.Y. Zavalij, N.A. Chernova, J. Mater. Chem. 15 (2005) 3362.

[141] H.D. Liu, G. Yang, X.F. Zhang, P. Gao, L. Wang, J.H. Fang, J. Pinto, X.F. Jiang, J. Mater. Chem. 22 (2012) 11039.

[142] P.S. Herle, B. Ellis, N. Coombs, L.F. Nazar, Nat. Mater. 3 (2004) 147.

[143] J. Molenda, A. Stoklosa, T. Bak, Solid State Ionics 36 (1989) 53.

[144] M. Nishizawa, T. Ise, H. Koshika, T. Itoh, I. Uchida, Chem. Mater. 12 (2000) 1367.

[145] C.X. Huang, D.D. Chen, Y.Y. Huang, Y.L. Guo, Electrochim. Acta 100 (2013) 1.

[146] M.M. Ren, Z. Zhou, Y.Z. Li, X.P. Gao, J. Yan, J. Power Sources 162 (2006) 1357.

[147] L.L. Zhang, X. Zhang, Y.M. Sun, W. Luo, X.L. Hu, X.J. Wu, Y.H. Huang, J. Electrochem. Soc. 158 (2011) A924.

[148] M. Park, X.C. Zhang, M.D. Chung, G.B. Less, A.M. Sastry, J. Power Sources 195 (2010) 7904.

[149] S. Lee, S.S. Park, J. Phys. Chem. C 116 (2012) 25190.

[150] P.P. Prosini, M. Lisi, D. Zane, M. Pasquali, Solid State Ionics 148 (2002) 45.

[151] X.H. Rui, D.H. Sim, C. Xu, W.L. Liu, H.T. Tan, K.M. Wong, H.H. Hng, T.M. Lim, Q.Y. Yan, RSC Adv. 2 (2012) 1174.

[152] K.M. Shaju, G.V.S. Rao, B.V.R. Chowdari, Electrochim. Acta 48 (2003) 2691.

[153] X.H. Rui, N. Ding, J. Liu, C. Li, C.H. Chen, Electrochim. Acta 55 (2010) 2384.

[154] H. Huang, T. Faulkner, J. Barker, M.Y. Saidi, J. Power Sources 189 (2009) 748.

[155] A.P. Tang, X.Y. Wang, G.R. Xu, Z.H. Zhou, H.D. Nie, Mater. Lett. 63 (2009) 1439.

[156] T. Jiang, W.C. Pan, J. Wang, X.F. Bie, F. Du, Y.J. Wei, C.Z. Wang, G. Chen, Electrochim. Acta 55 (2010) 3864.

[157] Y.Q. Qiao, X.L. Wang, J.Y. Xiang, D. Zhang, W.L. Liu, J.P. Tu, Electrochim. Acta 56 (2011) 2269.

[158] Y.Q. Qiao, X.L. Wang, Y.J. Mai, J.Y. Xiang, D. Zhang, C.D. Gu, J.P. Tu, J. Power Sources 196 (2011) 8706.

[159] W.F. Mao, J. Yan, H. Xie, Z.Y. Tang, Q. Xu, Electrochim. Acta 88 (2013) 429.

[160] N. Bockenfeld, A. Balducci, J. Power Sources 235 (2013) 265.

[161] Y.H. Chen, Y.M. Zhao, X.N. An, J.M. Liu, Y.Z. Dong, L. Chen, Electrochim. Acta 54 (2009) 5844.

[162] M.M. Ren, Z. Zhou, X.P. Gao, W.X. Peng, J.P. Wei, J. Phys. Chem. C 112 (2008) 5689.

[163] A.Q. Pan, J. Liu, J.G. Zhang, W. Xu, G.Z. Cao, Z.M. Nie, B.W. Arey, S.Q. Liang, Electrochem. Commun. 12 (2010) 1674.

[164] F. Teng, Z.H. Hu, X.H. Ma, L.C. Zhang, C.X. Ding, Y. Yu, C.H. Chen, Electrochim. Acta 91 (2013) 43.

[165] Y. Zhang, Q.Y. Huo, P.P. Du, L.Z. Wang, A.Q. Zhang, Y.H. Song, Y. Lv, G.Y. Li, Synth. Met. 162 (2012) 1315.

[166] X.C. Zhou, Y.M. Liu, Y.L. Guo, Electrochim. Acta 54 (2009) 2253.

[167] L.J. Wang, X.C. Zhou, Y.L. Guo, J. Power Sources 195 (2010) 2844.

[168] P. Fu, Y.M. Zhao, Y.Z. Dong, X.N. An, G.P. Shen, Electrochim. Acta 52 (2006) 1003.

[169] Y.Z. Li, X. Liu, J. Yan, Electrochim. Acta 53 (2007) 474.

[170] X.J. Zhu, Y.X. Liu, L.M. Geng, L.B. Chen, H.X. Liu, M.H. Cao, Solid State Ionics 179 (2008) 1679.

[171] G. Yang, G. Wang, W.H. Hou, J. Phys. Chem. B 109 (2005) 11186.

[172] S. Beninati, L. Damen, M. Mastragostino, J. Power Sources 180 (2008) 875.

[173] Y. Qiao, X.L. Hu, Y. Liu, Y.H. Huang, Electrochim. Acta 63 (2012) 118.

[174] K.J. Rao, B. Vaidhyanathan, M. Ganguli, P.A. Ramakrishnan, Chem. Mater. 11 (1999) 882.

[175] G. Yang, H.D. Liu, H.M. Ji, Z.Z. Chen, X.F. Jiang, J. Power Sources 195 (2010) 5374.

[176] G. Yang, H.M. Ji, H.D. Liu, B. Qian, X.F. Jiang, Electrochim. Acta 55 (2010) 3669.

[177] H.P. Liu, S.F. Bi, G.W. Wen, X.G. Teng, P. Gao, Z.J. Ni, Y.M. Zhu, F. Zhang, J. Alloys Compd. 543 (2012) 99.

[178] D. Choi, P.N. Kumta, J. Power Sources 163 (2007) 1064.

[179] H. Liu, Y.P. Wu, E. Rahm, R. Holze, H.Q. Wu, J. Solid State Electrochem. 8 (2004) 450.

[180] L.L. Hench, J.K. West, Chem. Rev. 90 (1990) 33.

[181] Y.Z. Li, Z. Zhou, M.M. Ren, X.P. Gao, J. Yan, Electrochim. Acta 51 (2006) 6498.

[182] L.J. Wang, H.B. Liu, Z.Y. Tang, L. Ma, X.H. Zhang, J. Power Sources 204 (2012) 197.

[183] L.L. Zhang, Y. Li, G. Peng, Z.H. Wang, J. Ma, W.X. Zhang, X.L. Hu, Y.H. Huang, J. Alloys Compd. 513 (2012) 414.

[184] Y. Tang, B.H. Zhong, X.D. Guo, H. Liu, Y.J. Zhong, X.A. Nie, H. Tang, Acta Phys.-Chim. Sin. 27 (2011) 869.

[185] J. Yan, W. Yuan, H. Xie, Z.Y. Tang, W.F. Mao, L. Ma, Mater. Lett. 71 (2012) 1.

[186] W. Yuan, J. Yan, Z.Y. Tang, O. Sha, J.M. Wang, W.F. Mao, L. Ma, J. Power Sources 201 (2012) 301.

[187] Y.Z. Li, Z. Zhou, X.P. Gao, J. Yan, Electrochim. Acta 52 (2007) 4922.

[188] H. Wang, Y.J. Li, C.H. Huang, Y.D. Zhong, S.Q. Liu, J. Power Sources 208 (2012) 282.

[189] X.H. Rui, C. Li, J. Liu, T. Cheng, C.H. Chen, Electrochim. Acta 55 (2010) 6761.

[190] L.J. Wang, Z.Y. Tang, L. Ma, X.H. Zhang, Electrochem. Commun. 13 (2011) 1233.

[191] M.R. Gao, Y.F. Xu, J. Jiang, S.H. Yu, Chem. Soc. Rev. 42 (2013) 2986.

[192] J.J. Chen, M.J. Vacchio, S.J. Wang, N. Chernova, P.Y. Zavalij, M.S. Whittingham, Solid State Ionics 178 (2008) 1676.

[193] H. Yu, X.H. Rui, H.T. Tan, J. Chen, X. Huang, C. Xu, W.L. Liu, D.Y.W. Yu, H.H. Hng, H.E. Hoster, Q.Y. Yan,

Nanoscale 5 (2013) 4937.

[194] X.J. Zhang, W.H. Shi, J.X. Zhu, D.J. Kharistal, W.Y. Zhao, B.S. Lalia, H.H. Hng, Q.Y. Yan, ACS Nano 5 (2011) 2013.

[195] M.K. Devaraju, I. Honma, Adv. Energy Mater. 2 (2012) 284.

[196] C.X. Chang, J.F. Xiang, X.X. Shi, X.Y. Han, L.J. Yuan, J.T. Sun, Electrochim. Acta 54 (2008) 623.

[197] H.W. Liu, C.X. Cheng, X.T. Huang, J.L. Li, Electrochim. Acta 55 (2010) 8461.

[198] Y.Q. Qiao, J.P. Tu, J.Y. Xiang, X.L. Wang, Y.J. Mai, D. Zhang, W.L. Liu, Electrochim. Acta 56 (2011) 4139.

[199] W.C. Duan, Z. Hu, K. Zhang, F.Y. Cheng, Z.L. Tao, J. Chen, Nanoscale 5 (2013) 6485.

[200] G.L. Messing, S.C. Zhang, G.V. Jayanthi, J. Am. Ceram. Soc. 76 (1993) 2707.

[201] Y.N. Ko, J.H. Kim, S.H. Choi, Y.C. Kang, J. Power Sources 211 (2012) 84.

[202] Y.N. Ko, H.Y. Koo, J.H. Kim, J.H. Yi, Y.C. Kang, J.H. Lee, J. Power Sources 196 (2011) 6682.

[203] Y.N. Ko, J.H. Kim, Y.J. Hong, Y.C. Kang, Mater. Chem. Phys. 131 (2011) 292.

[204] O.A. Shlyakhtin, Y.S. Yoon, S.H. Choi, Y.J. Oh, Electrochim. Acta 50 (2004) 505.

[205] S.J. Shi, J.P. Tu, Y.Y. Tang, Y.X. Yu, Y.Q. Zhang, X.L. Wang, J. Power Sources 221 (2013) 300.

[206] V. Palomares, A. Goni, L.G. de Muro, I. de Meatza, M. Bengoechea, O. Miguel, T. Rojo, J. Power Sources 171 (2007) 879.

[207] C. Wang, H.M. Liu, W.S. Yang, J. Mater. Chem. 22 (2012) 5281.

[208] Y.Q. Qiao, X.L. Wang, Y.J. Mai, X.H. Xia, J. Zhang, C.D. Gu, J.P. Tu, J. Alloys Compd. 536 (2012) 132.

[209] S. Cavaliere, S. Subianto, I. Savych, D.J. Jones, J. Roziere, Energy Environ. Sci. 4 (2011) 4761.

[210] M. Inagaki, Y. Yang, F.Y. Kang, Adv. Mater. 24 (2012) 2547.

[211] A. Greiner, J.H. Wendorff, Angew. Chem. Int. Ed. 46 (2007) 5670.

[212] Z.X. Dong, S.J. Kennedy, Y.Q. Wu, J. Power Sources 196 (2011) 4886.

[213] L.W. Ji, Z. Lin, M. Alcoutlabi, O. Toprakci, Y.F. Yao, G.J. Xu, S.L. Li, X.W. Zhang, RSC Adv. 2 (2012) 192.

[214] O. Toprakci, L.W. Ji, Z. Lin, H.A.K. Toprakci, X.W. Zhang, J. Power Sources 196 (2011) 7692.

[215] Q.Q. Chen, T.T. Zhang, X.C. Qiao, D.Q. Li, J.W. Yang, J. Power Sources 234 (2013) 197.

[216] C.H. Chen, E.M. Kelder, P. vanderPut, J. Schoonman, J. Mater. Chem. 6 (1996) 765.

[217] C.H. Chen, E.M. Kelder, M.J.G. Jak, J. Schoonman, Solid State Ionics 86-8 (1996) 1301.

[218] X.F. Li, C.L. Wang, J. Mater. Chem. A 1 (2013) 165.

[219] Y. Yu, C.H. Chen, J.L. Shui, S. Xie, Angew. Chem. Int. Ed. 44 (2005) 7085.

[220] L. Wang, L.C. Zhang, I. Lieberwirth, H.W. Xu, C.H. Chen, Electrochem. Commun. 12 (2010) 52.

[221] C.X. Chang, J.F. Xiang, X.X. Shi, X.Y. Han, L.J. Yuan, J.T. Sun, Electrochim. Acta 53 (2008) 2232.

[222] Y.J. Li, L. Hong, J.Q. Sun, F. Wu, S. Chen, Electrochim. Acta 85 (2012) 110.

[223] J.S. Huang, L. Yang, K.Y. Liu, Mater. Lett. 66 (2012) 196.

[224] K. Nathiya, D. Bhuvaneswari, Gangulibabu, N. Kalaiselvi, Mater. Res. Bull. 47 (2012) 4300.

[225] K. Nagamine, T. Honma, T. Komatsu, J. Power Sources 196 (2011) 9618.

[226] X.L. Li, W.X. He, Z.H. Xiao, F.F. Peng, J.J. Chen, J. Solid State Electrochem. 17 (2013) 1991.

[227] J. Su, X.L. Wu, J.S. Lee, J. Kim, Y.G. Guo, J. Mater. Chem. A 1 (2013) 2508.

[228] J.C. Zheng, X.H. Li, Z.X. Wang, H.J. Guo, Q.Y. Hu, W.J. Peng, J. Power Sources 189 (2009) 476.

[229] W.F. Mao, J. Yan, H. Xie, Z.Y. Tang, Q. Xu, J. Power Sources 237 (2013) 167.

[230] X.H. Rui, N. Yesibolati, C.H. Chen, J. Power Sources 196 (2011) 2279.

[231] L.F. Fei, W. Lu, L. Sun, J.P. Wang, J.B. Wei, H.L.W. Chan, Y. Wang, RSC Adv. 3 (2013) 1297.

[232] X.P. Zhang, H.J. Guo, X.H. Li, Z.X. Wang, L. Wu, Electrochim. Acta 64 (2012) 65.

[233] L.A. Wang, X.Q. Jiang, X. Li, X.Q. Pi, Y. Ren, F. Wu, Electrochim. Acta 55 (2010) 5057.

[234] Q. Kuang, Y.M. Zhao, J. Power Sources 216 (2012) 33.

[235] L.L. Ge, C.X. Han, L.P. Ni, J. Zhang, Y.L. Tao, Q.B. Yu, Y.H. Shen, A.J. Xie, L. Zhu, Y.P. Zhang, Solid State Sci. 14 (2012) 864.

[236] J.S. Huang, L. Yang, K.Y. Liu, Mater. Chem. Phys. 128 (2011) 470.

[237] Z.Y. Chen, C.S. Dai, G. Wu, M. Nelson, X.G. Hu, R.X. Zhang, J.S. Liu, J.C. Xia, Electrochim. Acta 55 (2010) 8595.

[238] T. Jiang, F. Du, K.J. Zhang, Y.J. Wei, Z. Li, C.Z. Wang, G. Chen, Solid State Sci. 12 (2010) 1672.

[239] T. Jiang, C.Z. Wang, G. Chen, H. Chen, Y.J. Wei, X. Li, Solid State Ionics 180 (2009) 708.

[240] X.H. Rui, N. Yesibolati, S.R. Li, C.C. Yuan, C.H. Chen, Solid State Ionics 187 (2011) 58.

[241] X. Zhang, S.Q. Liu, K.L. Huang, S.X. Zhuang, J. Guo, T. Wu, P. Cheng, J. Solid State Electrochem. 16 (2012) 937.

[242] W.F. Mao, J. Yan, H. Xie, Y. Wu, Z.Y. Tang, Q. Xu, Mater. Res. Bull. 47 (2012) 4527.

[243] Y.Q. Qiao, X.L. Wang, Y. Zhou, J.Y. Xiang, D. Zhang, S.J. Shi, J.P. Tu, Electrochim. Acta 56 (2010) 510.

[244] Y.Q. Qiao, J.P. Tu, X.L. Wang, C.D. Cu, J. Power Sources 199 (2012) 287.

[245] Y.Q. Qiao, J.P. Tu, Y.J. Mai, L.J. Cheng, X.L. Wang, C.D. Gu, J. Alloys Compd. 509 (2011) 7181.

[246] J.W. Wang, X.F. Zhang, J. Liu, G.L. Yang, Y.C. Ge, Z.J. Yu, R.S. Wang, X.M. Pan, Electrochim. Acta 55 (2010) 6879.

[247] L.L. Zhang, G. Peng, G. Liang, P.C. Zhang, Z.H. Wang, Y. Jiang, Y.H. Huang, H. Lin, Electrochim. Acta 90 (2013) 433.

[248] B. Huang, X.P. Fan, X.D. Zheng, M. Lu, J. Alloys Compd. 509 (2011) 4765.

[249] J.W. Wang, J. Liu, G.L. Yang, X.F. Zhang, X.D. Yan, X.M. Pan, R.S. Wang, Electrochim. Acta 54 (2009) 6451.

[250] Y.Q. Qiao, J.P. Tu, X.L. Wang, D. Zhang, J.Y. Xiang, Y.J. Mai, C.D. Gu, J. Power Sources 196 (2011) 7715.

[251] X.Y. Du, W. He, X.D. Zhang, Y.Z. Yue, H. Liu, X.G. Zhang, D.D. Min, X.X. Ge, Y. Du, J. Mater. Chem. 22 (2012) 5960.

[252] L.X. Yuan, Z.H. Wang, W.X. Zhang, X.L. Hu, J.T. Chen, Y.H. Huang, J.B. Goodenough, Energy Environ. Sci. 4 (2011) 269.

[253] A.Q. Pan, D.W. Choi, J.G. Zhang, S.Q. Liang, G.Z. Cao, Z.M. Nie, B.W. Arey, J. Liu, J. Power Sources 196 (2011) 3646.

[254] C.W. Sun, S. Rajasekhara, Y.Z. Dong, J.B. Goodenough, ACS Appl. Mater. Inter. 3 (2011) 3772.

[255] A.K. Geim, Science 324 (2009) 1530.

[256] C.N.R. Rao, A.K. Sood, K.S. Subrahmanyam, A. Govindaraj, Angew. Chem. Int. Ed. 48 (2009) 7752.

[257] M.J. Allen, V.C. Tung, R.B. Kaner, Chem. Rev. 110 (2010) 132.

[258] G. Kucinskis, G. Bajars, J. Kleperis, J. Power Sources 240 (2013) 66.

[259] S. Han, D.Q. Wu, S. Li, F. Zhang, X.L. Feng, Small 9 (2013) 1173.

[260] S.H. Lee, V. Sridhar, J.H. Jung, K. Karthikeyan, Y.S. Lee, R. Mukherjee, N. Koratkar, I.K. Oh, ACS Nano 7 (2013) 4242.

[261] S. Bai, X.P. Shen, RSC Adv. 2 (2012) 64.

[262] H.D. Liu, P. Gao, J.H. Fang, G. Yang, Chem. Commun. 47 (2011) 9110.

[263] Y. Jiang, W.W. Xu, D.D. Chen, Z. Jiao, H.J. Zhang, Q.L. Ma, X.H. Cai, B. Zhao, Y.L. Chu, Electrochim. Acta 85 (2012) 377.

[264] L. Zhang, S.Q. Wang, D.D. Cai, P.C. Lian, X.F. Zhu, W.S. Yang, H.H. Wang, Electrochim. Acta 91 (2013) 108.

[265] J.F. Zhu, R.S. Yang, K.L. Wu, Ionics 19 (2013) 577.

[266] B. Pei, Z.Q. Jiang, W.X. Zhang, Z.H. Yang, A. Manthiram, J. Power Sources 239 (2013) 475.

[267] X.H. Rui, D.H. Sim, K.M. Wong, J.X. Zhu, W.L. Liu, C. Xu, H.T. Tan, N. Xiao, H.H. Hng, T.M. Lim, Q.Y. Yan, J. Power Sources 214 (2012) 171.

[268] W.J. Hao, H.H. Zhan, J. Yu, Mater. Lett. 83 (2012) 121.

[269] K.L. Wu, J.P. Yang, Mater. Res. Bull. 48 (2013) 435.

[270] L. Zhang, X.L. Wang, J.Y. Xiang, Y. Zhou, S.J. Shi, J.P. Tu, J. Power Sources 195 (2010) 5057.

[271] J. Zhai, M.S. Zhao, D.D. Wang, Y.Q. Qiao, J. Alloys Compd. 502 (2010) 401.

[272] L.L. Zhang, G. Liang, G. Peng, F. Zou, Y.H. Huang, M.C. Croft, A. Ignatov, J. Phys. Chem. C 116 (2012) 12401.

[273] S.D. Xun, J. Chong, X.Y. Song, G. Liu, V.S. Battaglia, J. Mater. Chem. 22 (2012) 15775.

[274] L.J. Wang, X.X. Li, Z.Y. Tang, X.H. Zhang, Electrochem. Commun. 22 (2012) 73.

[275] L.J. Wang, C.Q. Du, Z.Y. Tang, X.H. Zhang, Q. Xu, Electrochim. Acta 98 (2013) 218.

[276] T. Jiang, Y.J. Wei, W.C. Pan, Z. Li, X. Ming, G. Chen, C.Z. Wang, J. Alloys Compd. 488 (2009) L26.

[277] Y. Jin, C.P. Yang, X.H. Rui, T. Cheng, C.H. Chen, J. Power Sources 196 (2011) 5623.

[278] J. Chong, S.D. Xun, X.Y. Song, P. Ridgway, G. Liu, V.S. Battaglia, J. Power Sources 200 (2012) 67.

[279] J. Chong, S.D. Xun, X.Y. Song, G. Liu, V.S. Battaglia, Nano Energy 2 (2013) 283.

[280] T.F. Yi, J. Shu, Y.R. Zhu, A.N. Zhou, R.S. Zhu, Electrochem. Commun. 11 (2009) 91.

[281] Y. Zhang, Q.Y. Huo, Y. Lv, L.Z. Wang, A.Q. Zhang, Y.H. Song, G.Y. Li, H.L. Gao, T.C. Xia, H.C. Dong, J. Alloys Compd. 542 (2012) 187.

[282] S.Q. Liu, S.C. Li, K.L. Huang, B.L. Gong, G. Zhang, J. Alloys Compd. 450 (2008) 499.

[283] J.N. Son, G.J. Kim, M.C. Kim, S.H. Kim, V. Aravindan, Y.G. Lee, Y.S. Lee, J. Electrochem. Soc. 160 (2013) A87.

[284] Q. Kuang, Y.M. Zhao, X.N. An, J.M. Liu, Y.Z. Dong, L. Chen, Electrochim. Acta 55 (2010) 1575.

[285] M. Bini, S. Ferrari, D. Capsoni, V. Massarotti, Electrochim. Acta 56 (2011) 2648.

[286] W.L. Wu, J. Liang, J. Yan, W.F. Mao, J. Solid State Electrochem. 17 (2013) 2027.

[287] J.S. Huang, L. Yang, K.Y. Liu, Y.F. Tang, J. Power Sources 195 (2010) 5013.

[288] D.J. Ai, K.Y. Liu, Z.G. Lu, M.M. Zou, D.Q. Zeng, J. Ma, Electrochim. Acta 56 (2011) 2823.

[289] J.H. Yao, S.S. Wei, P.J. Zhang, C.Q. Shen, K.F. Aguey-Zinsou, L.B. Wang, J. Alloys Compd. 532 (2012) 49.

[290] W. Yuan, J. Yan, Z.Y. Tang, O. Sha, J.M. Wang, W.F. Mao, L. Ma, Electrochim. Acta 72 (2012) 138.

[291] C. Deng, S. Zhang, S.Y. Yang, Y. Gao, B. Wu, L. Ma, B.L. Fu, Q. Wu, F.L. Liu, J. Phys. Chem. C 115 (2011) 15048.

[292] S. Zhang, Q. Wu, C. Deng, F.L. Liu, M. Zhang, F.L. Meng, H. Gao, J. Power Sources 218 (2012) 56.

[293] J.N. Son, S.H. Kim, M.C. Kim, G.J. Kim, V. Aravindan, Y.G. Lee, Y.S. Lee, Electrochim. Acta 97 (2013) 210.

[294] J. Yan, W. Yuan, Z.Y. Tang, H. Xie, W.F. Mao, L. Ma, J. Power Sources 209 (2012) 251.

[295] Q. Kuang, Y.M. Zhao, Z.Y. Liang, J. Power Sources 196 (2011) 10169.

[296] Q.Q. Chen, X.C. Qiao, Y.B. Wang, T.T. Zhang, C. Peng, W.M. Yin, L. Liu, J. Power Sources 201 (2012) 267.

[297] S.K. Zhong, L.T. Liu, J.Q. Liu, J. Wang, J.W. Yang, Solid State Commun. 149 (2009) 1679.

[298] K. Nathiya, D. Bhuvaneswari, Gangulibabu, D. Nirmala, N. Kalaiselvi, RSC Adv. 2 (2012) 6885.

[299] S.Y. Yang, S. Zhang, B.L. Fu, Q. Wu, F.L. Liu, C. Deng, J. Solid State Electrochem. 15 (2011) 2633.

[300] C.S. Dai, Z.Y. Chen, H.Z. Jin, X.G. Hu, J. Power Sources 195 (2010) 5775.

[301] A.R. Cho, J.N. Son, V. Aravindan, H. Kim, K.S. Kang, W.S. Yoon, W.S. Kim, Y.S. Lee, J. Mater. Chem. 22 (2012) 6556.

[302] Y.X. Tang, X.H. Rui, Y.Y. Zhang, T.M. Lim, Z.L. Dong, H.H. Hng, X.D. Chen, Q.Y. Yan, Z. Chen, J. Mater. Chem.

A 1 (2013) 82.

[303] D. Yang, Y.P. Zhou, X.H. Rui, J.X. Zhu, Z.Y. Lu, E. Fong, Q.Y. Yan, RSC Adv. 3 (2013) 14960.

[304] D. Yang, J.X. Zhu, X.H. Rui, H.T. Tan, R. Cai, H.E. Hoster, D.Y.W. Yu, H.H. Hng, Q.Y. Yan, ACS Appl. Mater. Inter. 5 (2013) 1093.

[305] D.H. Sim, X.H. Rui, J. Chen, H.T. Tan, T.M. Lim, R. Yazami, H.H. Hng, Q.Y. Yan, RSC Adv. 2 (2012) 3630.

[306] C. Xu, Y. Zeng, X.H. Rui, J.X. Zhu, H.T. Tan, A. Guerrero, J. Toribio, J. Bisquert, G. Garcia-Belmonte, Q.Y. Yan, J. Phys. Chem. C 117 (2013) 17462.

[307] L.Q. Mai, S. Li, Y.F. Dong, Y.L. Zhao, Y.Z. Luo, H.M. Xu, Nanoscale 5 (2013) 4864.

[308] R. von Hagen, A. Lepcha, X.F. Song, W. Tyrra, S. Mathur, Nano Energy 2 (2013) 304.

[309] L. Zhang, H.F. Xiang, Z. Li, H.H. Wang, J. Power Sources 203 (2012) 121.

Figure and Table Captions:

Table 1 The effect of carbon coating on the electrochemical performance of LVP cathodes.

Table 2 The effect of ion-doping on the electrochemical performance of LVP cathodes.

Fig. 1 Schematic illustration of a lithium ion battery employing graphite as anode and layered $LiCoO_2$ as cathode.

Fig. 2 Comparison of operating voltage and practical capacity of various cathode materials presently used in lithium ion batteries.

Fig. 3 Polyhedral representation of the structure of rhombohedral (A) and monoclinic (B) $Li_3V_2(PO_4)_3$.

Fig. 4 The electrochemical voltage-composition curves of $Li_3V_2(PO_4)_3$ in the voltage ranges of 3.0-4.8 (A) and 3.0-4.3 (B) V *vs.* Li/Li^+.

Fig. 5 (A) Possible Li-ion migration pathways in LVP. Reproduced with permission from [149]. (B) Lithium diffusion coefficients of LVP as determined by CV, GITT and EIS techniques. Reproduced with permission from [153].

Fig. 6 The morphology of LVP cathode materials prepared by different methods. (A) Solid-state reaction. Reproduced with permission from [123]. (B) Sol-gel chemistry. Reproduced with permission from [156]. (C) Hydrothermal method. Reproduced with permission from [199]. (D) Spray pyrolysis. Reproduced with permission from [202]. (E) Freeze-drying method. Reproduced with permission from [207]. (F) Electrospinning. Reproduced with permission from [215]. (G) Electrostatic spray deposition. Reproduced with permission from [220]. (H) Rheological phase reaction. Reproduced with permission from [221]. (I) Ionothermal method. Reproduced with permission from [226].

Fig. 7 TEM images showing a carbon layer (*ca*. 30-40 nm) uniformly coated on LVP particle surface, and good connection of LVP particles through the carbon network. Reproduced with permission from [249].

Fig. 8 The effects of different carbon content (A), carbon sources (B), and sintering temperatures (C) on the electrochemical properties of carbon coated LVP. (A-C) were reproduced with permission from [189], [137], and [157], respectively.

Fig. 9 (A) Schematic illustration of the formation mechanism of LVP-NC@NPCM@rGO. (B) SEM image. (C) HRTEM image. (D) Electron transfer pathways throughout the whole binder-free LVP-NC@NPCM@rGO electrode and corresponding optical image (inset). (E) Comparison of discharge capacities of binder-free LVP-NC@NPCM@rGO and normal LVP/C electrodes at various current rates between 3.0 and 4.3 V *vs.* Li/Li^+. Inset: cycling performance of LVP-NC@NPCM@rGO electrode at 50 C. (F) Rate capability of binder-free LVP-NC@ NPCM@rGO electrode in a wider voltage window (3.0-4.8 V *vs.* Li/Li^+) and corresponding cycling performance at 30 C (inset). Reproduced with permission from [267].

Fig. 10 (A) HRTEM images of LVP/(Ag + C), and (B) the first charge/discharge curves of LVP, LVP/C, and LVP/(Ag + C) electrodes at 0.1 C. Reproduced with permission from [270]. (C) TEM image of LVP/C-2Si, and (D) rate capability of pristine LVP/C, LVP/C-1Si, LVP/C-2Si, and LVP/C-3Si electrodes. Reproduced with permission from [272]. (E) TEM image of G-LVPO synthesized at 900 ^oC, and (F) cycling performance of bare LVP and G-LVPO at 1 C. Reproduced with permission from [273].

Fig. 11 (A) Cycling performance of $Li_3V_{2-x}Fe_x(PO_4)_3/C$ at 0.2 C. Reproduced with permission from [146]. (B) Rate capability of $Li_3V_{2-x}Cr_x(PO_4)_3/C$. Reproduced with permission from [161]. (C) Long-term cycling performance of $Li_3V_{2-2x}Ti_xMg_x(PO_4)_3/C$ at 0.5 C. Reproduced with permission from [291]. (D) Cycling performance of $Li_{3-x}Na_xV_2(PO_4)_3/C$ at 1 C. Reproduced with permission from [296]. (E) Cycling performance of the pristine LVP/C and $Li_3V_2(PO_4)_{2.88}Cl_{0.12}/C$ at 5 and 8 C (inset is the 10^{th} charge-discharge profiles of $Li_3V_2(PO_4)_{2.88}Cl_{0.12}/C$ at 5 and 8 C). Reproduced with permission from [294]. (F) Cycling performance of $Li_3V_{1.98}Al_{0.02}(PO_4)_{2.99}Cl_{0.01}/C$ at 0.05 and 15 C. Reproduced with permission from [293].

Fig. 12 Schematic illustration of facile electron and lithium transport in LVP nanospheres with continuous carbon network and carbon coating layer (A) and top cross-section view (B). SEM image (C) and corresponding HRTEM image (D) of the sample prepared with 20 wt% PEG-4000. (E) Its cycling performance at 5 C rate for 5000 cycles. Reproduced with permission from [307].

Fig. 13 (A) High magnification SEM image of LVP/C nanobelts. (B) Discharge/charge curves of LVP/C nanobelts at various C-rates. Reproduced with permission from [253].

Fig. 14 Schematic illustration of three different electrodes (nanofiber self-supported electrode, film electrodes based on

dispersed nanofibers and nanoparticles). Reproduced with permission from [308].

Fig. 15 SEM (A), TEM (B, C), and HRTEM (D) images of LVP/C nanoplates. Reproduced with permission from [158].

Fig. 16 (A) Schematic illustration of the porous LVP/C composite for facile electrolyte penetration. (B) TEM image of porous precursor. (C) Cycling performance of porous LVP/C from 10 to 100 C between 3.0 and 4.8 V *vs.* Li/Li^+. Reproduced with permission from [309].